buildings

MDPI

Article

Unlocking Rooftop Cooling Potential: An Experimental Investigation of the Thermal Behavior of Cool Roof and Green Roof as Retrofitting Strategies in Hot–Humid Climate

Tengfei Zhao [1,*], Kwong Fai Fong [2] and Tin Tai Chow [2]

[1] College of Architecture and Urban Planning, Beijing University of Technology, 100 Pingleyuan, Chaoyang District, Beijing 100124, China
[2] Department of Architecture and Civil Engineering, City University of Hong Kong, Hong Kong, China
* Correspondence: tfzhao@bjut.edu.cn

Abstract

Cool roof and green roof have been acknowledged as effective heat mitigation strategies for fighting against the urban heat island (UHI). However, empirical data in hot–humid climate are still insufficient. Experimental conventional, cool and green roofs (three types) were established to comprehensively investigate the thermal performances in Hong Kong under typical summer conditions, as retrofitting strategies for an office building. The holistic vertical thermal behavior was investigated. The comparative cooling potentials were assessed. The results reveal a "vertical thermal sequence" in peak temperatures of each substrate layer for the conventional, cool and green roofs on a sunny day. However, local reversion in the thermal sequence may occur on a rainy day. Green roof-plot C (GR_C) demonstrates the highest thermal damping effect, followed by plot B (GR_B), A (GR_A) and the cool roof (CR) in summer. On a sunny day, the thermal dampening effectiveness of the substrates in the three green roofs is consistent: drainage > soil > water reservoir > root barrier. The holistic vertical thermal profiling was constructed in a high-rise office context in Hong Kong. The diurnal temperature profiles indicate all roof systems could effectively attenuate the temperature fluctuations. The daily maximum surface temperature reduction (SDMR) was introduced for cooling potential characterization of the cool roof and green roofs with multiple vegetation types. On a sunny day, the cool roof and green roofs all showed significant cooling potential. SDMR on the concrete tile of the best performing system was GR_C (26 °C), followed by GR_B (22.4 °C), GR_A (20.7 °C) and CR (13.3 °C), respectively. The SDMR on the ceiling ranked as GR_C, GR_B, GR_A and CR, with 2.9 °C, 2.4 °C, 2.1 °C and 2.1 °C, separately. On a rainy day, the cooling effect was still present but greatly diminished. A critical insight of a "warming effect at the ceiling" of the green roof was revealed. This research offers critical insights for unlocking rooftop cooling potential, endorsing cool roof and green roof as pivotal solutions for sustainable urban environments.

Keywords: cool roof; green roof; field measurements; hot-humid climate; thermal performances; cooling potential; urban heat island mitigation

Check for updates

Academic Editor: Adrian Pitts

Received: 17 December 2025
Revised: 30 December 2025
Accepted: 10 January 2026
Published: 15 January 2026

Copyright: © 2026 by the authors. Licensee MDPI, Basel, Switzerland. This article is an open access article distributed under the terms and conditions of the Creative Commons Attribution (CC BY) license.

1. Introduction

Urbanization involves concentration of the population, loss of natural surfaces and expansion of living space above and below ground. All of these factors alter the balance of radiation, heat and water, generating a climate typical of urban areas—the "urban

climate" [1]. The 'urban heat island (UHI)', which is an evident modification that affects local climate [2,3], commonly exists in urban areas. It is a phenomenon whereby cities become warmer than the surrounding suburbs [4]. Elevated temperatures in cities have adverse implications for energy demand [5–7], air pollution [8], greenhouse gases [9] and human health [10]. The challenges they pose will continue to grow with future climate change. As such, heat islands are widely recognized as stumbling blocks in the sustainable pathways of metropolitan areas. Previous research efforts have permitted the development of UHI mitigation strategies [11]. The proposed strategies that are most studied in the literature and adopted by cities are the use of high-albedo materials and green spaces [12–14]. A previous study shows that the roof area fraction was estimated to vary from 20% to 25% for less or more dense cities [15]. By considering the highly valuable urban land and application potential of roof area, mitigation strategies focusing on building rooftops have been increasingly promoted to create cooling benefits.

Nowadays, cool roof and green roof have been acknowledged as effective heat mitigation strategies. Cool roof, which utilizes high-albedo materials, is also known as reflective roof [16,17]. Corresponding to higher solar reflection, lower solar radiation is absorbed [18]. Green roof, which is partially or completely covered with vegetation, is also known as living roof [19,20]. Green roof can be classified as intensive, semi-intensive and extensive types, according to their substrate depth and plants used [21,22]. Intensive (over 15–40 cm) and semi-intensive (over 12–25 cm) green roofs could bring more significant ecological and environmental benefits, but the thick and heavy substrate limits its application [23,24]. Roof greening is dominated by the extensive type (6–20 cm), using a relatively thin and light-weight substrate [25]. When applied in building retrofitting, extensive green roof is more appropriate as these solutions do not overload the existing structure [26]. Their cooling performance is mainly from the combined effects of shading and evapotranspiration [27]. A thorough understanding of the thermal performance of cool roof and green roof is crucial for their effective application.

Thermal benefits have received the bulk of researchers' attention, covering varied climate types. Those benefits in fighting against UHI are mainly associated with temperature regulation and energy consumption. Lowered roof surface temperature and diurnal temperature fluctuation could reduce the direct heating of ambient air. Simultaneously, it denotes less building heat gain and building energy consumption, especially in summer [28,29]. Specifically, green roof in different climates (temperate, hot–humid, hot–dry) showed significant cooling potential, covering many metropolitan cities in the world [30–42]. Dry climate has the highest median cooling effect (3 °C), while hot–humid climate presents the lowest median cooling potential (1 °C). Green roof contributes a median surface temperature reduction of 28 °C and 30 °C, respectively. Cool roof performance with different types of surface coatings in different climatic zones for buildings was summarized [43–48]. The average roof surface temperature reduction ranges from 1.4 to 4.7 °C in different climate zones (temperate, tropical, hot–dry, composite, warm–humid) via using cool roof technology. The average energy saving is expressed from 15 to 35.7%. In general, field measurements in different climates show that the daily maximum surface temperature of cool and green roofs can be 10–30 °C lower than that of conventional roofs [18,49,50]. Many simulation findings are consistent with field measurements [51–53]. However, in situ measurements and empirical data of thermal performances of different roofs in specific climates are still insufficient. Although the provided results are very useful, it is quite difficult to extrapolate them to other conditions and make accurate predictions.

The influencing factors regarding system thermal performance have been identified. The thermal and energy benefits caused by the implementation of cool roof vary mainly as a

function of climatic conditions, albedo of the roof surface and characteristics of the building (building type and construction) [26,54]. Besides local climate conditions, green roof's cooling performance varies according to system characteristics and the building's physical properties [55]. Green roof system characteristics, including plant biomass structure and leaf area index, substrate thickness and moisture content, design and thickness of drainage layer, exert multiple influences on the thermal performance [56–60]. Intrinsic building factors such as building type, thermal capacitance and insulation property correlate [61,62]. However, few studies quantifying the cooling benefits of cool roof can be found in countries outside the U.S. and Europe; detailed experimental and simulation data in various climatic conditions are still needed. Whilst the possible thermal benefits of green roof are generally a well investigated area, existent literature is scarce in evaluating substrates. The role of the substrate layers (including drainage) in the thermal process is lacking. Hence, besides evaluating the total cooling performance, temperature changes across the substrates, roof fabric and underneath indoor space could be studied holistically in a comprehensive experimental design in hot–humid climate.

A thermal performance comparison helps to clarify the climate adaptability and utilization priority. A series of simulations conducted in Marid, Spain, revealed that green roof decreased the annual building needs for heating and cooling by 1.2%, while cool roof (albedo = 0.7) contributed to decrease the needs by 0.4% [63]. An experiment carried out in an office building in New York, U.S., showed that substitution of cool roof (albedo = 0.6) with green roof resulted in energy savings of about 40–110% [64]. Studies carried out in U.S. and Europe cities found that the results depended on vegetation characteristics and fabric properties. In insulated buildings, cool roofs (albedo = 0.7) performed best in cold climates, while in non-insulated buildings, green roof performed best in warm climates [65]. Reflective roofs presented lower cooling energy consumption than buildings with high LAI green roofs. Buildings equipped with green roofs of high leaf area index (LAI) values presented much lower energy consumption for cooling than buildings with a low LAI value [52]. In tropical Singapore, the simulation results showed that, during peak periods (9 a.m. to 5 p.m.), cool roofs reduce heat gain by about 0.14 KWh/m^2 (8%), and green roofs mitigate considerably less to about 0.008 KWh/m^2 (0.4%). For the whole of a summer design day, cool and green roofs reduce heat gain by 15.53 (37%) and 13.14 (31%) KWh/m^2, respectively [38]. However, comparative studies on the cooling performance of cool roof and green roof are relatively limited. This can be attributed to significant differences in their fundamental principles, climatic adaptability, application scenarios and experimental complexity, which pose challenges in comparison.

Hong Kong is compounded by an inordinately hilly and rugged landform, with limited flat and easily developed land. The urban areas are highly concentrated and accommodate bulk population, resulting in a compact city [66]. Densely packed buildings and roads create limited open spaces. The urban heat island effects generally exist. The vertical city has abundant rooftops, denoting available spaces to ameliorate the urban heating [67]. Thus, urban Hong Kong has a huge potential to embrace roof retrofitting. Office buildings generate enormous building energy demand on air-conditioning to cool the indoor environment in summer in hot–humid climate [68,69]. Installing cool roof/green roof would unlock significant cooling potential. Empirical studies of thermal performances could promote the unlocking of the cooling potential in subtropical climate, as the results from other climates may not be directly applicable. Systematic and local comparative exploration in the hot–humid climate context is worth advancement to facilitate implementation of cool roof and green roof.

Above all, this study focuses on the deficiencies identified in the literature, and the primary research aim is to experimentally investigate the thermal performance of cool roof and green roof, as retrofitting strategies for office buildings, on typical weather conditions in hot–humid climate. The holistic vertical thermal profiling across multiple substrate layers (along the "outermost surface–substrate layer–roof ceiling" vertical profile) of cool roof and green roof in a high-rise office context in Hong Kong is presented on days representative of typical summer weather conditions. The cooling potential of cool roof and green roof with multiple vegetation types is characterized and compared.

2. Study Area and Method

2.1. Study Area

Hong Kong is located on the southeast coast of China, with latitude 22°15′ N and longitude 114°10′ E. It has a monsoon-influenced humid–subtropical climate. The summer is long, tending towards hot and humid, with common sunny conditions, brief showers and thunderstorms. June to September are the hottest months of the year, with daily average temperatures varying from 27.6 °C (September) to 28.7 °C (July), daily maximum temperatures ranging from 30.2 °C (September) to 31.3 °C (July) and a relative humidity around 80%.

The experimental study was conducted at the City University of Hong Kong (CityU). Figure 1 shows the experimental sites that were constructed on the rooftop of the Amenities Building, which is a five-story office building. The whole green roof area covered about 245 m^2, and the experimental site took up 35 m^2. The site for field measurements was divided into three roughly equal plots, as shown in Figure 2. Three main types of vegetation were separately planted in the plots. The dimensions of the experimental site are illustrated in Figure 2. Underneath is an open-plan office space with no suspended ceiling, complemented by a few small rooms. The floor-to-floor height is 5 m. During the rooftop experimental period, the office space innovation was carried out in phases. Experimental data for the rooftop site was collected while the office space beneath was unoccupied, and the air-conditioning system was not in operation. Therefore, the cool roof and green roof experiments were not conducted simultaneously.

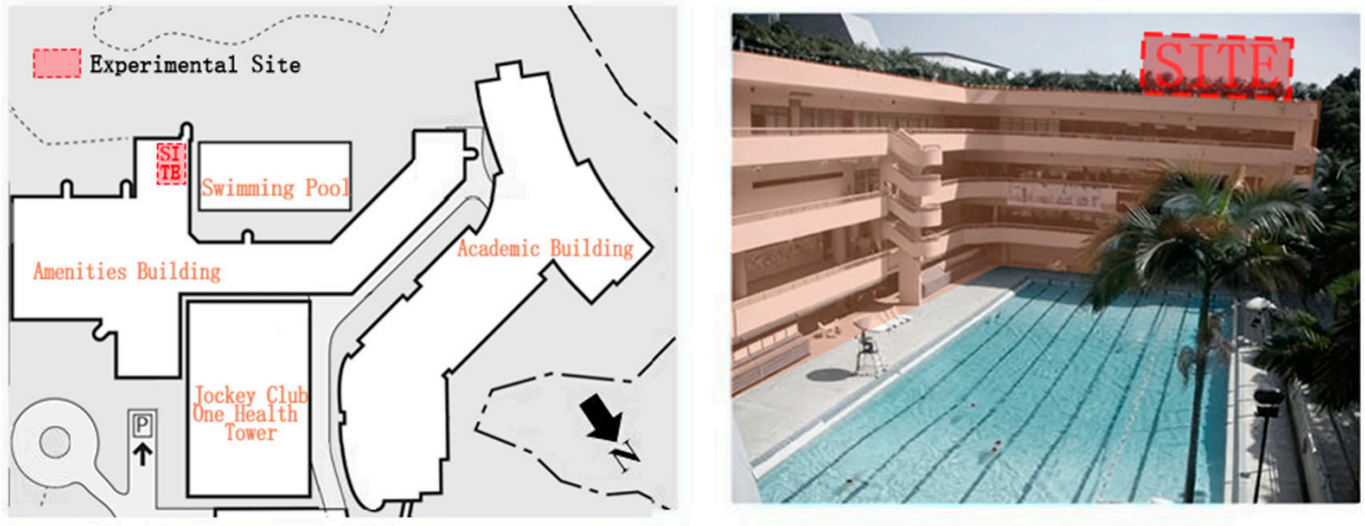


Figure 1. The location of the experimental site.

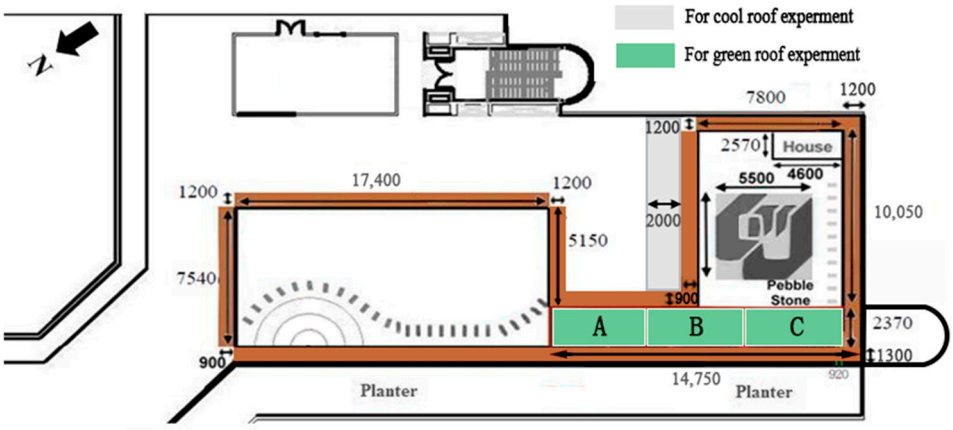


Figure 2. Dimensions (in millimeters) of the experimental site for the cool roof and green roof.

2.2. Experimental Design

This building configuration is a common construction design adopted in Hong Kong [70,71]. The roof of the experimental building was built using reinforced concrete, with a thermal insulation layer. The bare roof was constructed with five layers of conventional building materials that, from external to internal, are as follows:

- Concrete tiles;
- Mastic asphalt on black sheathing felt;
- Cement sand screed bedding;
- Polystyrene insulation layer;
- Concrete.

The external wall consists of four layers of building materials that, from external to internal, include the following:

- Mosaic tile;
- Sand plastering;
- Concrete;
- Gypsum plastering.

On top of the bare roof, the green roof was constructed referring to the typical design [72,73]. From top to bottom, the green roof system constituted six substrate layers, which were as follows:

- Vegetation layer;
- Light-weight soil;
- Water reservoir layer;
- Filter layer;
- Drainage layer;
- Root barrier layer;
- Water proofing membrane.

An automatic sprinkler irrigation system (Gardena, Ulm, Germany) was installed. The daily irrigation was scheduled at 9:00 and 15:00 separately. The substrate layers are shown in Figure 3 according to the construction process. As a high-density city, the plant selection for Hong Kong's rooftop greening system balances ecological benefits, climate adaptability and maintenance convenience. Three main types of vegetation commonly used with different heights, LAIs and distinct growth forms were selected and separately planted in each plot. The three green roof plots and corresponding physical properties of the vegetation are shown in Table 1. The planted vegetation types were Zoysia Japonica (plot A), Ophiopogon Jaburan (plot B) and Duranta Repens (plot C). The height of the

plants was measured using a measuring tape. Six sample locations for each plot were selected to determine the mean height value.



Figure 3. Construction layers of the green roof system.

Table 1. Green roof experimental plots and corresponding physical properties of the vegetation.

Experimental Plots of Green Roof	Plot A—Zoysia Japonica	Plot B—Ophiopogon Jaburan	Plot C—Duranta Repens
			
Height of plant	0.035 m	0.23 m	0.38 m

In May 2015, white paint was applied on the rooftop to establish the cool roof. The completed experimental sites of the conventional roof and the two HMSs on the roof can be seen in Figure 4.

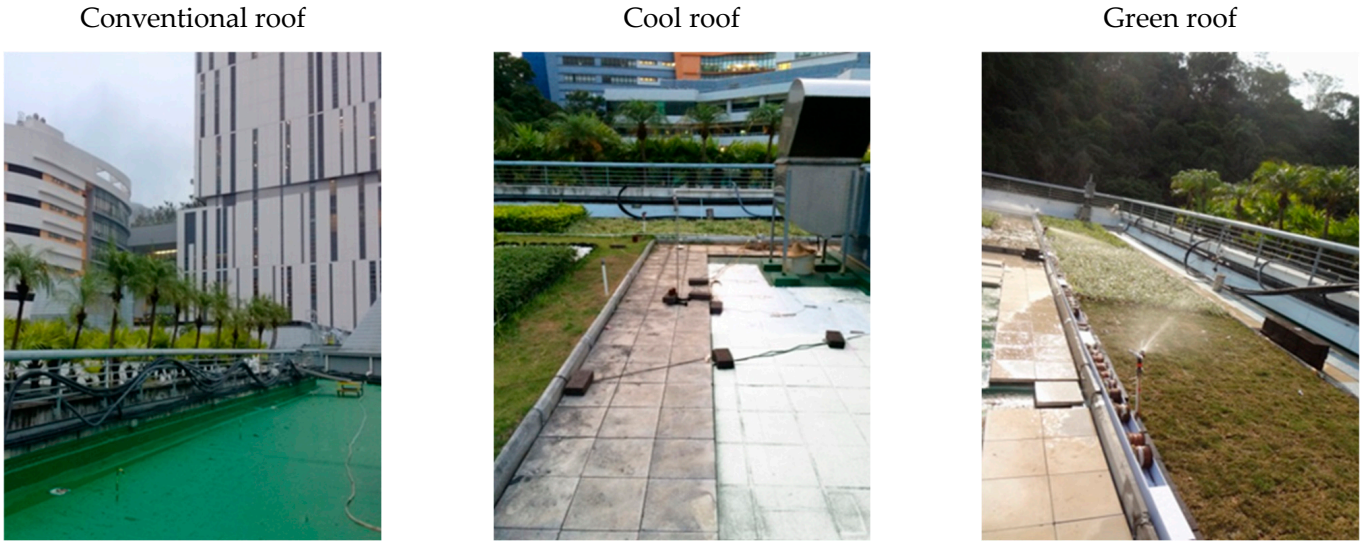


Figure 4. Completed experimental sites implemented with different roofing systems.

2.2.1. Local Weather Data

A weather station was also established and fitted with a set of sensors that were able to collect meteorological data. The local meteorological data needed to be collected, including solar radiation, ambient air temperature, relative humidity, wind speed, wind direction and rainfall. The established weather station is illustrated in Figure 5. The technical characteristics of the fitted sensors are listed in Table 2. The global solar radiation was measured by a CMP6 pyranometer (Kipp & Zonen, Delft, The Netherlands). The pyranometer tracks global solar radiation (total radiation), i.e., the sum of beam and diffuse solar radiation on a surface. The technical parameters are summarized in Table 3.

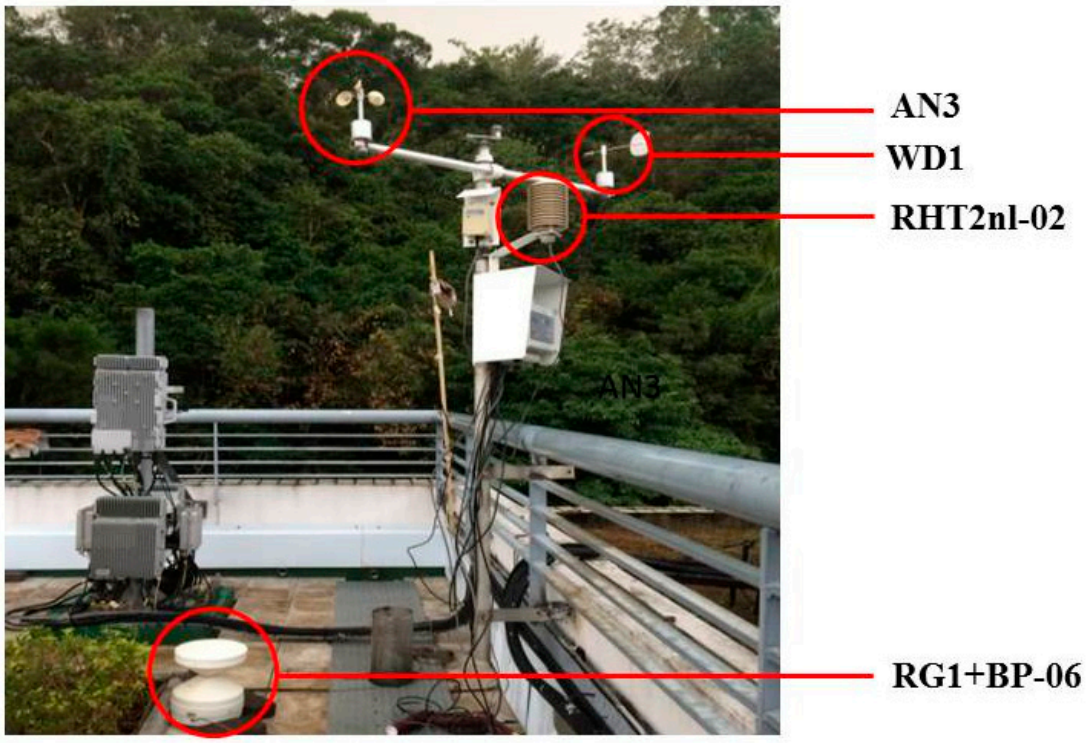


Figure 5. The established weather station for local meteorological data monitoring.

Table 2. The technical characteristics of the fitted sensors of the weather station (Delta-T WS-HP1).

Sensor	Sensor Brand and Type	Range	Accuracy and Unit
Air temperature	RHT2nl-02	−30–70 °C	±0.1 °C
Relative humidity	RHT2nl-02	0–100%	±2%
Wind speed	AN3	0.2–75 m/s	±0.1 m/s
Wind direction	WD1	0–358°	±0.3°
Rainfall	RG1 + BP-06	Max: 500 mm in 1 h	0.2 mm per tip

Table 3. The CMP6 pyranometer used for measurement and its specifications.

CMP6 Pyranometer	Specifications	Range
	Classification to ISO 9060:1990 [74]	First Class
	Spectral range (50% points)	285 to 2800 nm
	Sensitivity	(a) 15.89 μV/W/m^2 (upward) (b) 19.67 μV/W/m^2 (downward)
	Impedance	20 to 200 Ω
	Response time (63%)	<6 s
	Response time (95%)	<18 s
	Directional error (up to 80° with 1000 W/m^2 beam)	<20 W/m^2
	Detector type	Thermopile
	Operational temperature	−40 °C to +80 °C
	Maximum solar irradiance	2000 W/m^2
	Field of view	180°

Note: (a) was used for global solar radiation measurement; (a) and (b) were used for albedo measurement.

2.2.2. Albedo

The albedo of the roof surfaces was determined by measurement. There are three modes of albedo measurement: laboratory, field and remotely sensed modes. The present study focused on the third mode of measurement: using a portable apparatus for field measurement. The testing in this study was conducted in accordance with ASTM E1918 (Standard Test Method for Measuring Solar Reflectance of Horizontal and Low-Sloped Surfaces in the Field) [75] but using a dual pyranometer. This was mainly due to the possibility that the single pyranometer method could increase measurement error, since the incoming solar radiation and reflected solar radiation were not measured at the same time, especially on cloudy days.

In this study, two Kipp–Zonen CMP6 pyranometers were used to perform the measurement of solar reflectivity. The specifications are described in Table 3. One pyranometer faced upward, and the other faced downward. Incident global solar radiation (direct and diffuse solar radiation) was measured by the upward facing pyranometer, while reflected solar radiation from surfaces was measured by the downward facing pyranometer. The albedo was then computed as the ratio of reflected sunlight (up flux) to incident sunlight (down flux). General guidance for albedo measurement suggests that the sensor should be located at a height of 0.5 m [76,77]. A tripod was used to adjust the height of the downward pyranometer above different roof systems. The outputs of the pyranometers were recorded through a data logging system.

The measurement was carried out on a clear sunny day from 12:00 to 14:00, as shown in Figure 6. This measurement period was near solar noon, ensuring that the angle between the solar beam and the normal to the horizontal bed was always less than 45° and there was a relatively stable solar intensity. Two measurement locations were tested on each type of surface, with three repetitions performed within about three minutes at each measurement

point, simultaneously verifying that the span (max–min) of the three albedos did not exceed 0.01. The resulting data were then averaged into a single calculated albedo for every surface type. For each measurement, 30 s was allowed for the pyranometer to stabilize.

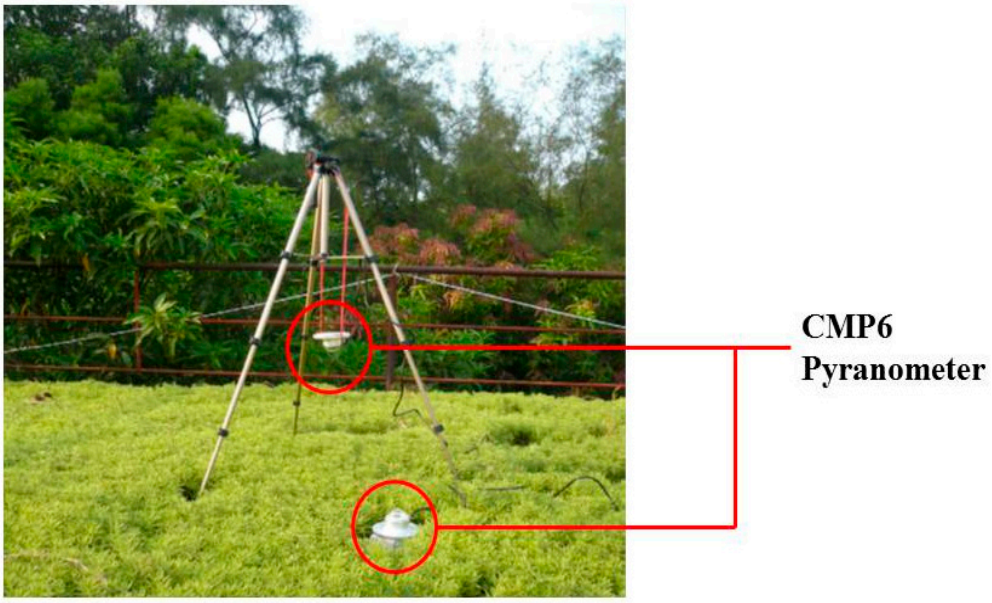


Figure 6. On-site measurement of albedo.

2.2.3. Surface Temperature

Arrays of temperature sensors (i.e., thermocouple) were installed at each layer interface of the substrates for monitoring time-varying temperatures. In Figure 7, for the bare roof, the sensors were fixed at the tile surface of the bare roof and underneath the surface of the bare roof (i.e., ceiling surface). Sensor locations for the cool roof were the same as the bare roof. For the green roof, the sensors were installed at the upper surface of the soil layer; the lower surface of the soil layer; the lower surface of the water reservoir layer; the lower surface of the drainage layer and the lower surface of the root barrier layer, respectively. Six temperature sensors were evenly installed at each layer interface. Three temperature sensors were installed on the top surfaces of the bare roof and cool roof, respectively. Corresponding to each type of roof, three sensors were fixed underneath the ceiling surfaces. As depicted in Figure 8, a T-type thermocouple, a miniature in-line plug and an in-line socket with an extension cable were employed for temperature measurement in this study. The specifications of the temperature sensor are given in Table 4.

Table 4. Specifications of the temperature sensor.

Name	Item	Specification
T-type thermocouple	Ranges of measurement	−200 °C to 350 °C
	Cable length	2 m
	Conductor insulation	Glass fiber
	Accuracy	±0.0075 T
	Reference brand/Model	RS Pro 6212209
PVC insulated flat pair extension cable	Insulation rating	−10 °C to 105 °C
	Conductor	7/0.2 mm
	Tolerance class	2
	Reference brand/Model	RS Pro 2363870

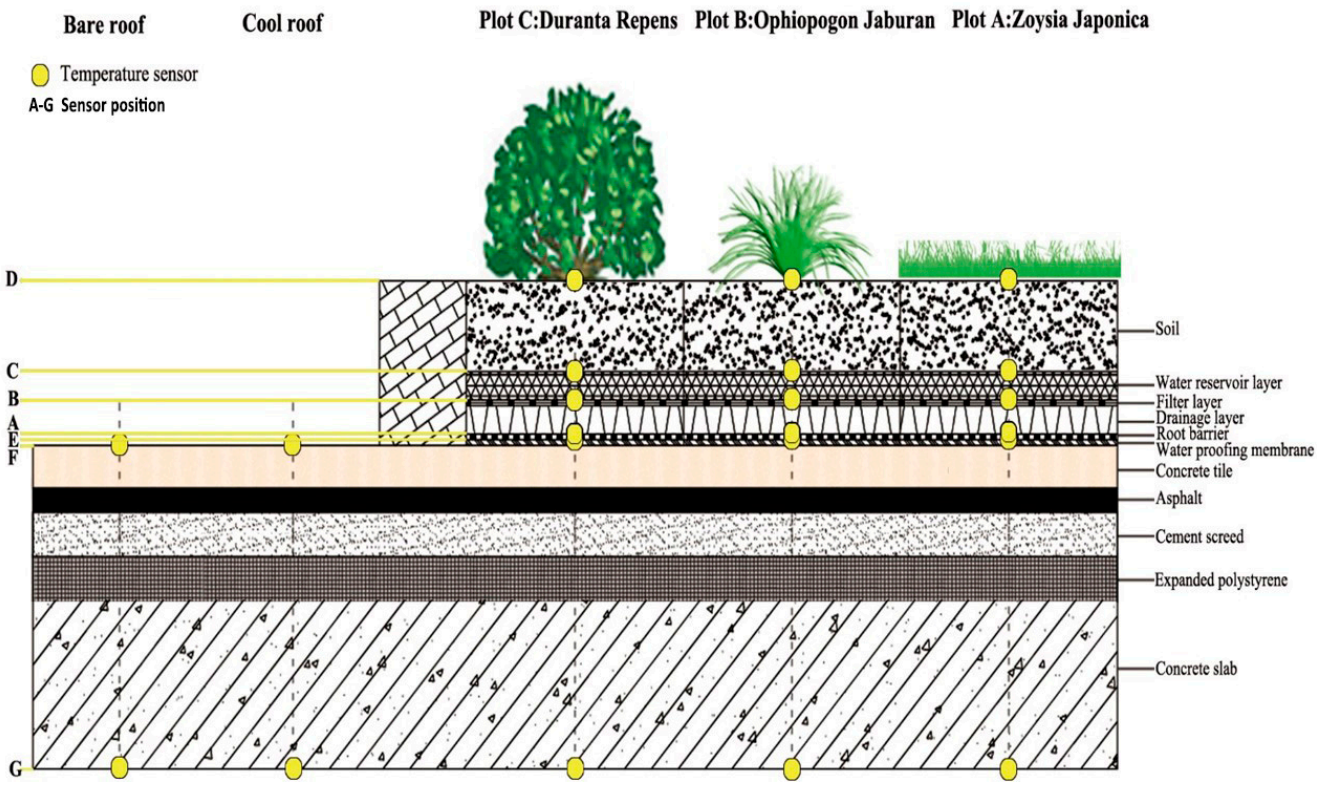


Figure 7. Schematic cross-sectional view of different roofing systems and positions of experimental sensors (A to G indicates sensor position).



Figure 8. T-type thermocouple connected with the extension cable.

2.2.4. Data Logging System

An Agilent Data Acquisition Switch Unit (34972A) and Armature Multiplexer Module (34901A) were employed for data logging and monitoring. This device had a set of input channels to acquire the data recorded by various sensors via signal cables automatically. The sensors connected to data loggers included thermocouples and pyranometers. The data logger received the information as an electrical signal and converted it into the desired magnitude. In this experiment, all of the data were recorded at a time interval of 5 min. Figure 9 illustrates the data logging system. The monitoring period lasted continuously for nine months for the green roof performance investigation, from April to December 2014. The field measurement of the cool roof was carried out during May–June 2015.



Figure 9. Agilent data acquisition unit.

3. Local Weather Conditions

Since the study of the cool roof was planned after that of the green roof, the performances of the cool roof and green roof on typical weather conditions were not presented on the same day. For the cool roof, the recorded surface temperatures on 17 June 2015 and 21 May 2015 were used to evaluate the performance on a typical summer sunny day and rainy day, respectively. On the other hand, 28 May 2014 and 8 May 2014 were selected as typical summer sunny and rainy days to analyze thermal performance of the green roof.

For the typical summer sunny and rainy days, the hourly profiles of global radiation and ambient air temperature are presented in Figure 10, while the relative humidity and rainfall data are described in Figure 11. Generally, the variation trends of ambient air temperature correlated well with the solar radiation. However, the fluctuation of relative humidity showed an opposite trend with incident solar energy. The climatic conditions on a summer sunny day can be characterized as strong solar radiation, high air temperature and high humidity. On a typical summer rainy day, due to reduced solar energy input and a large amount of precipitation, high relative humidity and relative lower ambient air temperature were obtained. In the following thermal performance assessment, the conventional roof served as a baseline to evaluate the cooling effect of the cool roof and green roof.

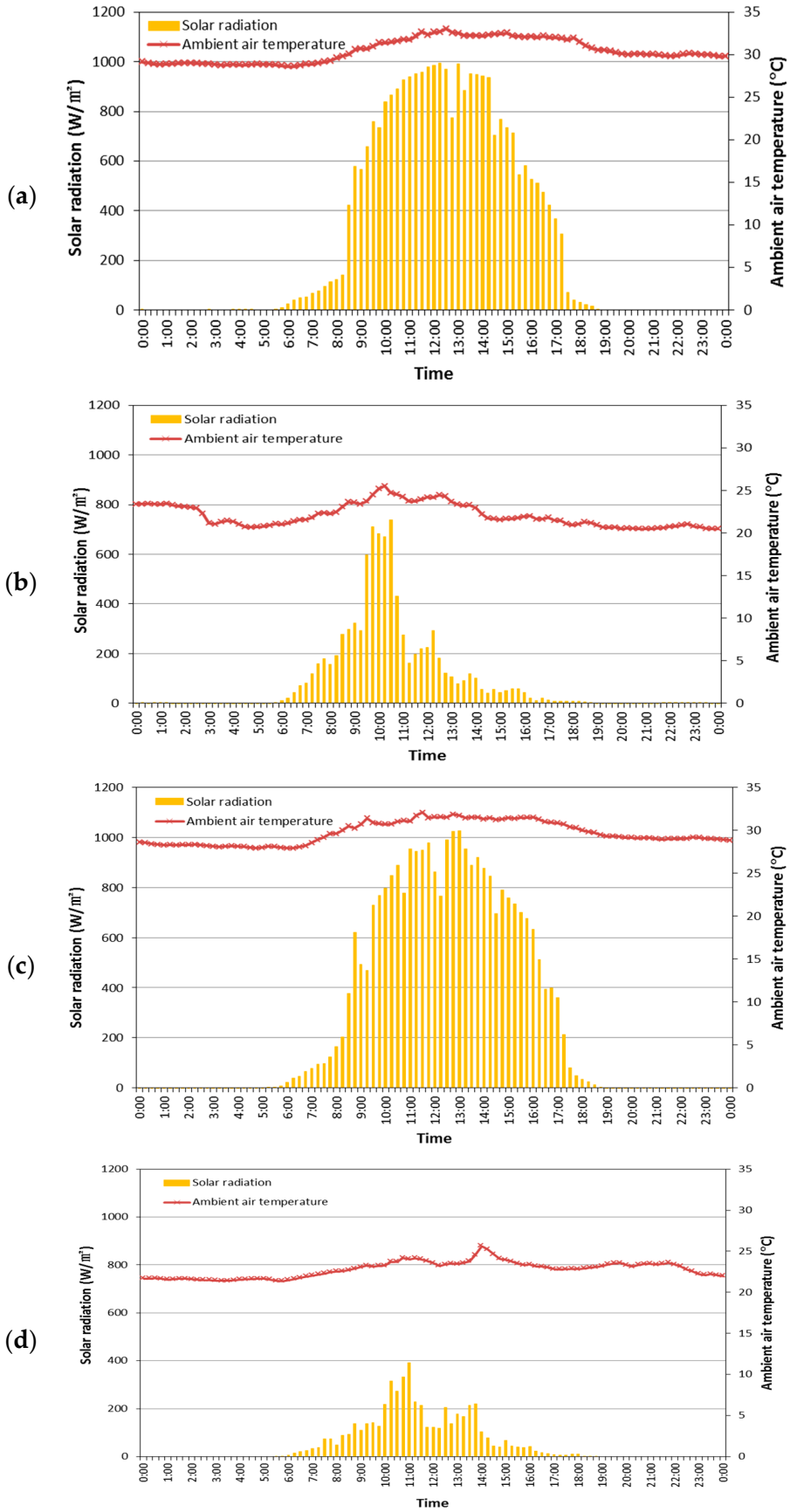


Figure 10. Hourly global horizontal solar radiation and ambient dry bulb air temperature for the typical summer (**a**) sunny day (17 June 2015) for the cool roof, (**b**) rainy day (21 May 2015) for the cool roof, (**c**) sunny day (28 May 2014) for the green roof and (**d**) rainy day (8 May 2014) for the green roof.

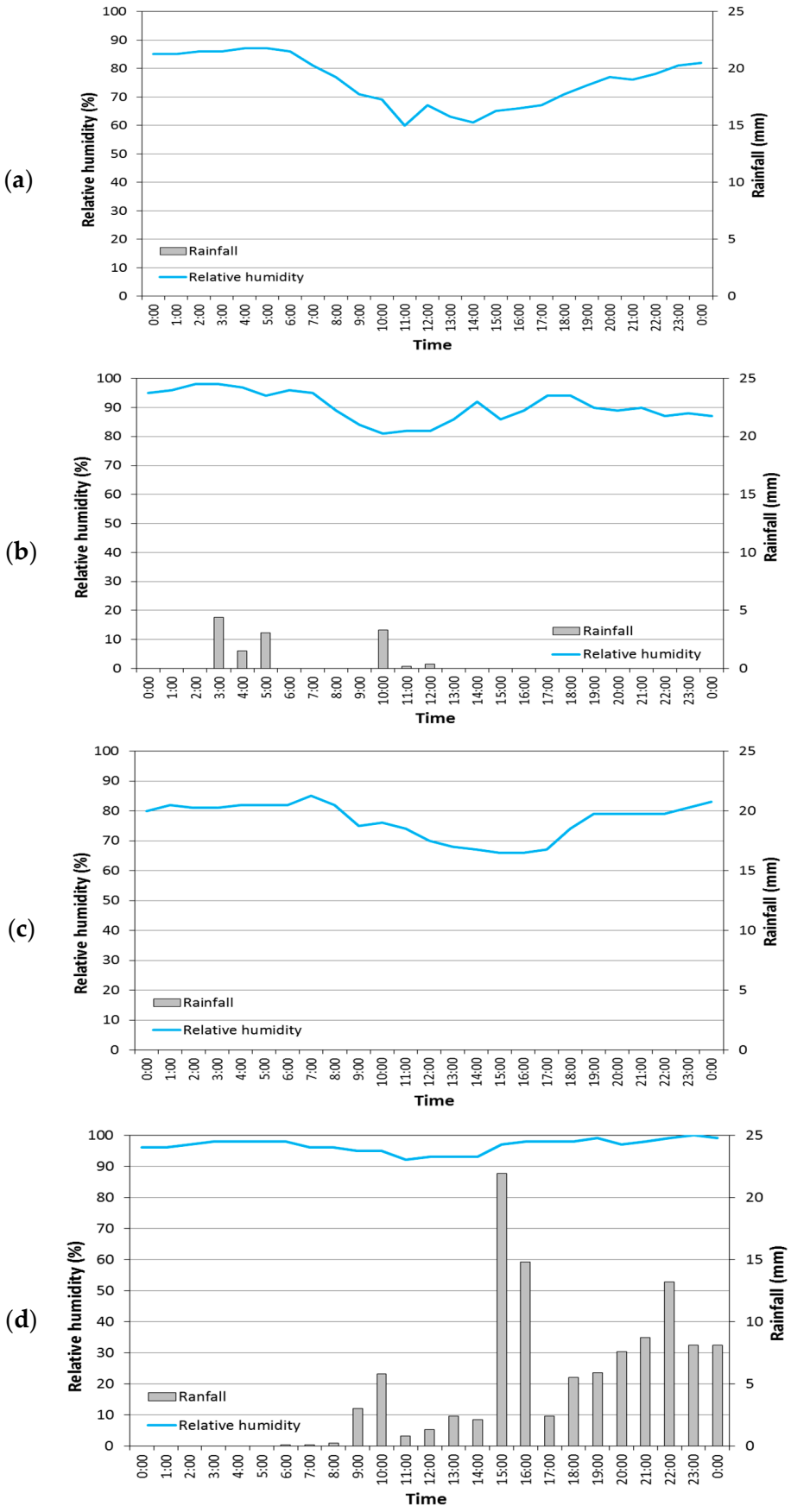


Figure 11. Hourly relative humidity and rainfall for the typical summer (**a**) sunny day (17 June 2015) for the cool roof, (**b**) rainy day (21 May 2015) for the cool roof, (**c**) sunny day (28 May 2014) for the green roof and (**d**) rainy day (8 May 2014) for the green roof.

4. The Vertical Thermal Behavior of the Cool Roof and Green Roof on Typical Summer Conditions

In order to enable normal office affairs to continue, a phased renovation plan was implemented. Therefore, the experimental periods of the cool roof and green roof were different. Diurnal temperature profiles on typical summer days for the conventional roof and cool roof were presented for analysis. Generally, the variations in rooftop surface temperature were closely related to the corresponding meteorological conditions in terms of ambient air temperature and solar radiation.

4.1. The Holistic Vertical Temperature Profiles Across the Roof Systems

4.1.1. Cool Roof

Summer Sunny Day

In Figure 12a, the rooftop surface temperature bottomed at about 07:00, with 27.8 °C. After that, the conventional rooftop surface temperature increased gradually and peaked at 55.6 °C at around 14:00. Then, the rooftop surface temperature experienced a declining trend and extended into the night with a gentle change. The diurnal fluctuation was closely related to the amount of incident solar radiation. The ceiling surface temperature demonstrated a relatively flat curve, with a constrained daily temperature variation at around 1.4 °C. The stable ceiling surface temperature that averaged 29.6 °C denoted good thermal barrier performance of the original roof construction. The concrete tile surface temperature was almost kept above the ceiling surface temperature.

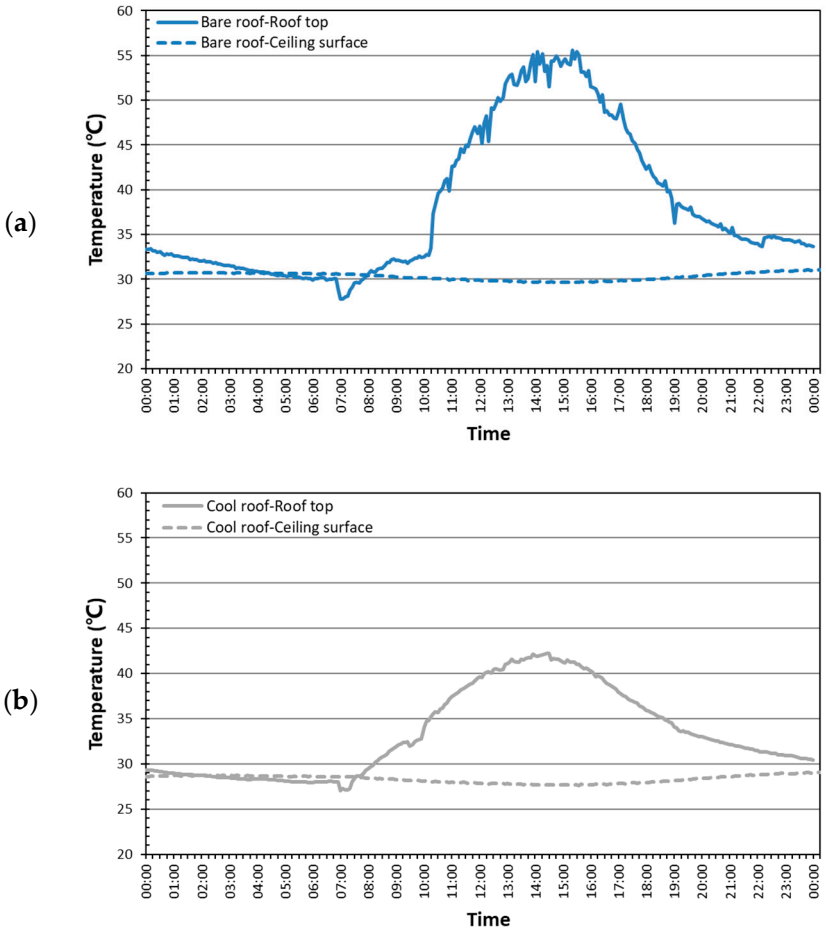


Figure 12. Diurnal vertical temperature profiles on a summer sunny day for (**a**) conventional roof and (**b**) cool roof.

Figure 12b shows the vertical temperature profiles of the cool roof. The fluctuation trends were generally the same, except for a lower peak temperature of the cool roof. Associated with the amount of incident solar radiation, the rooftop heated up gradually. Then, the maximum temperature was achieved at 42.3 °C at around 14:00 for the cool roof. The high albedo roof surface reduced the absorbed solar radiation and thus presented a lower surface temperature. The ceiling surface temperature was also generally flat, with limited diurnal variation less than 1.4 °C. The ceiling surface temperature kept at an average temperature of 28.3 °C. Less amount of absorbed solar radiation reduced the downward heat ingress. Therefore, the average ceiling surface temperature and variation range were all lower than the conventional roof. The cool roof demonstrated obvious cooling potential.

Summer Rainy Day

As illustrated in Figure 13a, the fluctuations of the rooftop surface temperature were similar to the variation in solar radiation and air temperature. Correlated to the lower amount of incident solar radiation during the rainy weather condition, the peak temperatures appeared early at about 10:30, with 30.1 °C for the conventional roof. The reduced amount of heat maintained the ceiling surface temperature nearly constant, with an average of about 24.3 °C. Different from sunny days, the concrete tile surface temperature was below the ceiling surface temperature from 1:00 to 8:50. After reaching the maximum, it started a descent stage and fell below the ceiling surface temperature again at around 16:05.

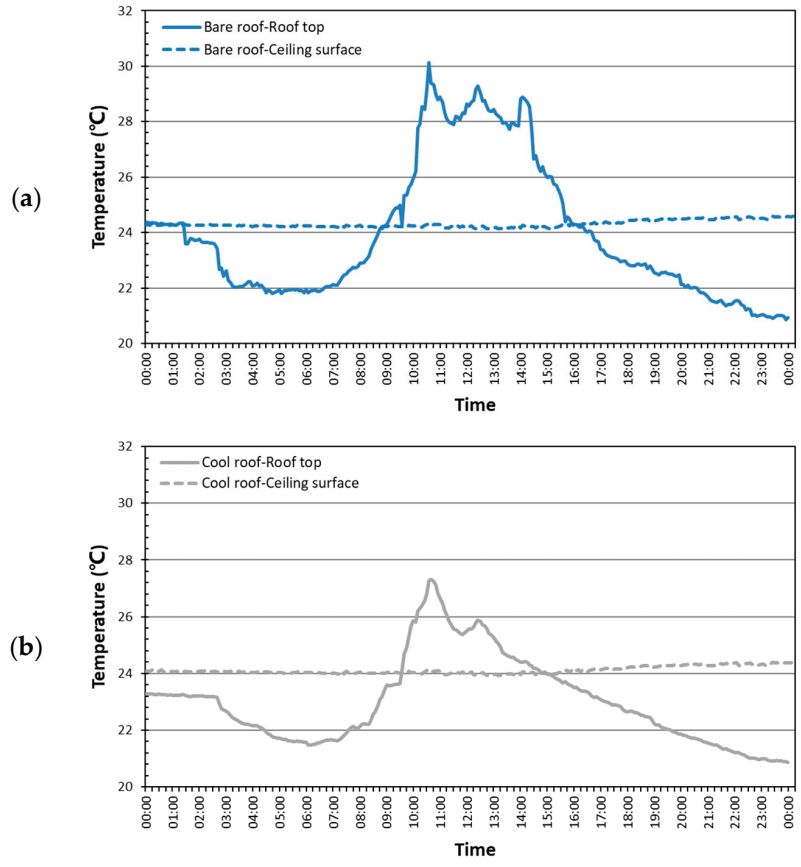


Figure 13. Diurnal vertical temperature profiles on a summer rainy day for (**a**) conventional roof and (**b**) cool roof.

Figure 13b shows the vertical temperature profiles of the cool roof. The fluctuation trends were generally the same, except for a lower peak temperature of the cool roof. The maximum temperature was achieved at 27.3 °C at around 10:30 for the cool roof. The high albedo reduced the absorbed solar radiation, and together with the evaporative cooling

effect of rainfall, the roof surface thus presented a lower surface temperature than the conventional roof. The ceiling surface temperature was also generally flat, with an average temperature of about 24.1 °C and diurnal variation less than 0.5 °C. The high albedo roof surface temperature kept below the ceiling surface temperature, except from 9:35 to 16:05. The cool roof demonstrated certain cooling potential even on a summer rainy day.

In general, the daily maximum temperature and diurnal variation ranges of the top substrate of the cool roof were obviously lower than those of the conventional roof due to its ability to reflect radiation and reduce heat absorption. Thus, it can be concluded that the cool roof showed definite heat mitigation potential during different weather conditions.

4.1.2. Green Roof

Diurnal temperature profiles on typical summer days for the conventional roof and green roofs were presented. In general, daily vertical temperature profiles for the conventional roof and three green roof plots also showed similar variation trends with ambient air temperature and solar radiation on the typical sunny and rainy days.

Summer Sunny Day

In Figure 14a, the roof surface temperature bottomed at around 07:00, with 27.8 °C. After sunrise, the temperature of the conventional roof surface increased obviously and was heated up to a maximum of 54.9 °C at around 13:30. Then, the absorbed heat in the concrete tiles was gradually released to the ambient air by convective heat transfer, which resulted in a surface temperature decrease. The decline trends became relatively flat during nighttime. In contrast, the ceiling surface temperature expressed a relatively flat curve, with limited diurnal variation less than 1.4 °C. The rather stable ceiling surface temperature (averaged at about 29.6 °C) indicated good thermal damping capacity of the conventional roof. The concrete surface temperature was nearly always higher than the ceiling surface temperature.

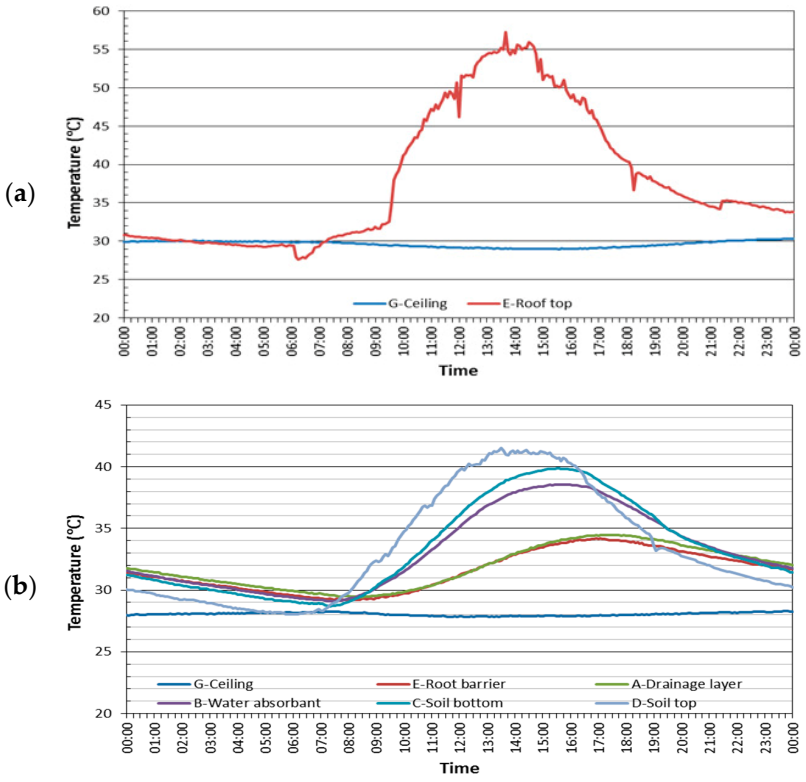


Figure 14. *Cont.*

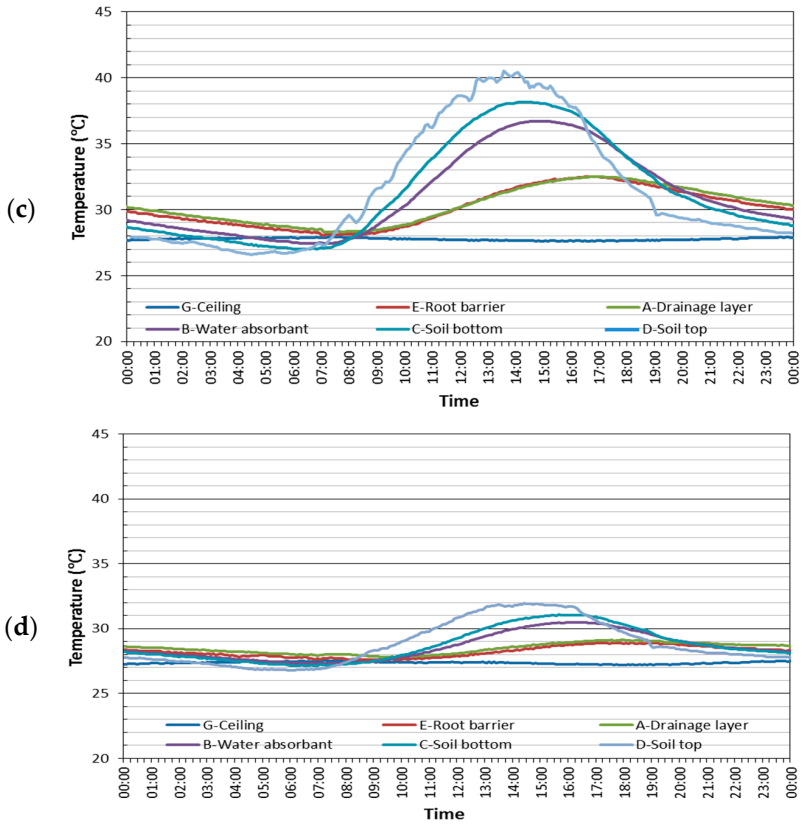


Figure 14. Diurnal vertical temperature profiles on a summer sunny day for (**a**) conventional roof, (**b**) green roof-plot A, (**c**) green roof-plot B and (**d**) green roof-plot C.

Figure 14b depicts the diurnal vertical temperature profiles for green roof-plot A (Zoysia Japonica). Associated with massive solar energy input in daytime, the substrate temperatures of each layer were raised up subsequently and peaked at mid-afternoon. The daily maximum temperature of the soil top was recorded at around 14:00, with about 41.5 °C, which was obviously lower than the conventional roof. This is primarily due to the shade of the vegetation, passive thermal insulation layer and active evapotranspiration effect. Moreover, the daily maximum temperature of each substrate demonstrated a "vertical thermal sequence". The temperature peaks gradually shifted towards a later time with lower values. In addition, the ceiling surface temperature was rather stable, kept at about 28.1 °C. The diurnal variation range was limited, constrained below 0.5 °C. It can be concluded that green roof-plot A presented a large heat mitigation potential compared to the conventional roof.

As shown in Figure 14c, the maximum temperatures of each substrate of green roof-plot B (Ophiopogon Jaburan) were decreased compared to plot A. The diurnal temperature profile of the soil top peaked at about 40.2 °C, which was lower by 1.3 °C compared to plot A. Corresponding to its denser vegetation cover, a larger amount of solar radiation did not reach the soil surface. Combined with more vigorous latent heat consumption due to evapotranspiration, a larger heat mitigation potential was demonstrated. The daily maximum temperatures of each substrate layer also displayed a "vertical thermal sequence". It was the same as plot A but with lower peak values, while the ceiling surface temperature hovered at around 27.8 °C, and the diurnal variation was below 0.3 °C. The average ceiling surface temperature and variation range were all lower than plot A. As such, green roof-plot B also presented clear thermal damping capacity.

In Figure 14d, the maximum temperature reduction of the soil top of green roof-plot C (Duranta Repens) is notable, registering as 32 °C, which denoted its advantage in passive

cooling. It remained the coolest in a diurnal cycle among the three green roof systems. The "vertical thermal sequence" also followed that of plots A and B but with limited amplitude. At the same time, the ceiling surface temperature recorded the lowest average value of about 27.4 °C compared to the conventional roof and green roof-plots A and B. Characterized by its vigorous growth and formation of tight green cover, green roof-plot C contributed the most effective cooling effects.

Summer Rainy Day

As illustrated in Figure 15a, subdued solar energy and abundant rainfall jointed together to cool the conventional roof surface on a summer rainy day. The daily maximum temperature was registered as 27.9 °C. The reduced amount of heat ingress maintained the ceiling surface temperature nearly constant, with an average of about 22.1 °C, which varied less than 0.48 °C. Different from sunny days, the concrete surface temperature kept below the ceiling surface from 0:00 to 8:00. After passing the maximum at around 14:00, it showed a declining trend and even fell below the ceiling surface temperature again at around 23:00.

Diurnal temperature fluctuations for the green roofs displayed similar curves to the conventional roof but with reduced ranges of swing. For green roof-plot A, in Figure 15b, the reduced solar radiation significantly dampened the temperature peaks. The recorded maximum temperature for the soil top was only 25.3 °C at around 14:00. Then, it experienced a sharp decrease, even falling below the temperature of the soil bottom and water absorbent layer at about 14:00–15:00. This was mainly because the rainwater provided an additional cooling effect to the substrates. The soil top inevitably played the role of a cooling front. After it dissipated heat downwards, its temperature soon declined below that of the soil bottom layer. The daily maximum temperature of each substrate also demonstrated a "vertical thermal sequence" as on the sunny days. Furthermore, the ceiling surface temperature was quite steady at around 22.5 °C and varied less than 0.24 °C. Even on a summer rainy day, green roof-plot A also showed certain heat mitigation capacity.

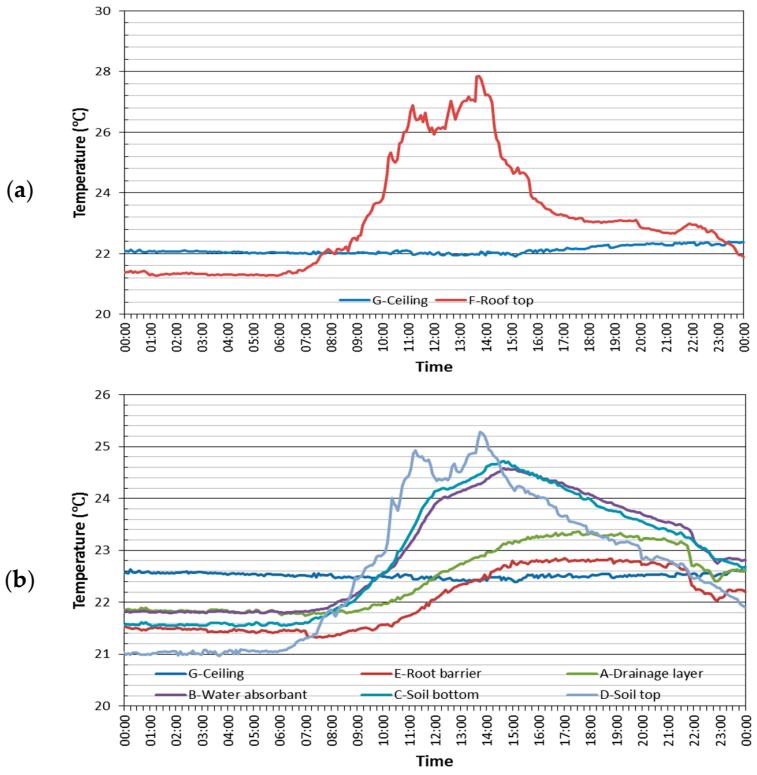


Figure 15. *Cont.*

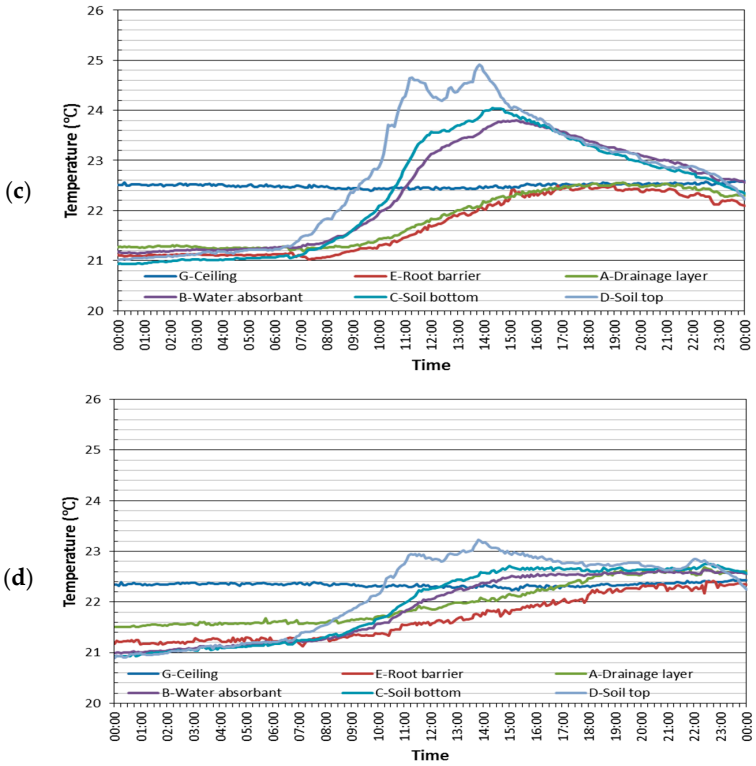


Figure 15. Diurnal vertical temperature profiles on a summer rainy day for (**a**) conventional roof, (**b**) green roof-plot A, (**c**) green roof-plot B and (**d**) green roof-plot C.

Similar variation trends can be found in Figure 15c. The daily maximum temperature of the soil top of plot B was about 24.9 °C, slightly lower than that of green roof-plot A. Dense vegetation covers could better reduce the influence of the atmosphere on the soil top temperature, resulting in small temperature variations in a 24 h period. After passing the peak, the soil top temperature gradually decreased and fell slightly below the soil bottom temperature until midnight. The "vertical thermal sequence" can also be observed among daily maximum temperatures of each substrate. It generally followed the sequence on a sunny day, except that the ceiling surface temperature may lie above some substrates. The temperature reversion can also be attributed to the rainwater cooling effects. The flat curve for the ceiling surface temperature only showed slight changes (less than 0.2 °C), with an average of about 22.4 °C. Thus, green roof-plot B could contribute to heat mitigation on a summer rainy day.

In Figure 15d, the recorded highest temperature for the soil top surface of green roof-plot C was 23.2 °C. Higher vegetation coverage weakened the environmental influences, resulting in a smaller diurnal temperature variation. The reversion of the ceiling surface temperature in the "vertical thermal sequence" can be observed more clearly. The mean ceiling surface temperature hovered at around 22.3 °C. As such, clear heat dissipation capacity was demonstrated by plot C.

4.2. The Vertical Thermal Sequence of Substrate Layers

4.2.1. Cool Roof

The diurnal maximum temperature and the occurrence time sequence are summarized in Table 5. On a summer sunny day, the temperature peaks were gradually shifted towards a later time with a lower value, resulting in a time-lag effect. We found the "vertical thermal sequence" in the daily maximum surface temperature of the substrate layers for the conventional roof and cool roof. The outermost layer, i.e., the concrete tile/high albedo rooftop, was heated up primarily, followed by the ceiling. The "vertical thermal sequence"

was closely related to the downward heat transfer. The white paint did not induce obvious time-lag heating, whilst the original roof construction denoted postponed heat ingress into indoor spaces. A similar condition can be found on a summer rainy day.

Table 5. Diurnal maximum temperature (°C) and occurrence time of the substrate layer for the cool roof on a summer sunny/rainy day.

Typical Weather Condition	Sensor Position	Conventional Roof		Cool Roof	
		Temp	Time	Temp	Time
Summer sunny day	Concrete tile/White paint	55.6	14:00	42.3	14:00
	Ceiling	31.1	23:45	29.1	23:45
Summer rainy day	Concrete tile/White paint	30.1	10:30	27.3	10:30
	Ceiling	24.6	23:25	24.4	23:25

4.2.2. Green Roof

The diurnal maximum temperatures of each substrate and the occurrence time sequence are summarized in Table 6. On a summer sunny day, the temperature peaks were gradually shifted towards a later time with a lower value, resulting in a time-lag effect. The observed "vertical thermal sequence" in the daily maximum temperatures of each substrate layer for the conventional roof and the three green roof systems was previously verified. The outermost layer played the role of a primary heating front, and the thermal sequence of the conventional roof followed concrete roof surface, ceiling, while the green roof followed soil top, soil bottom, water absorbent, drainage layer, root barrier, ceiling. The "vertical thermal sequence" correlated well with the downward heat transmission process. In response to the inherent features of multi-layer construction, they also denoted postponed heat ingress into indoor spaces. As a whole, the three green roof systems all demonstrated tangible heat mitigation potential on a summer sunny day.

Table 6. Diurnal maximum temperature (°C) and occurrence time of each substrate for four experimental plots on a summer sunny day.

Sensor Position	Conventional Roof		Green Roof-Plot A		Green Roof-Plot B		Green Roof-Plot C	
	Temp	Time	Temp	Time	Temp	Time	Temp	Time
Soil/Concrete top	54.9	13:30	41.5	13:30	40.2	13:35	32.0	14:25
Soil bottom	-	-	39.9	15:35	38.2	14:20	31.1	15:40
Water reservoir	-	-	38.6	15:35	36.7	15:05	30.5	16:25
Drainage	-	-	34.5	16:55	32.5	16:40	29.1	17:35
Root barrier	-	-	34.2	17:30	32.5	16:50	28.9	18:20
Ceiling	30.4	23:45	28.3	23:45	28.0	23:50	27.5	24:00

The diurnal maximum temperatures of each substrate and occurrence time sequence are summarized in Table 7. On a summer rainy day, the "vertical thermal sequence" of the daily peak temperatures of each substrate gained high similarity with that on a summer sunny day. However, the reversion caused by the ceiling surface temperatures can be found for green roof-plots B and C. For plot B, the ceiling surface temperature surpassed the temperatures of the drainage layer and root barrier layer, while for plot C, it mainly exceeded the temperature of the root barrier layer. Actually, this can be attributed to the process of heat transfer. Different from a sunny day, the outermost layer did not always absorb heat during the daytime. It also released heat to ambient in certain time periods.

It was exactly the uncertain condition of heat transfer that created the reversion in the thermal sequence, but generally, the three green roof systems all demonstrated certain heat mitigation potential on a summer rainy day.

Table 7. Diurnal maximum temperature (°C) and occurrence time of each substrate for four experimental plots on a summer rainy day.

Sensor Position	Conventional Roof		Green Roof-Plot A		Green Roof-Plot B		Green Roof-Plot C	
	Temp	Time	Temp	Time	Temp	Time	Temp	Time
Soil/Concrete top	27.9	13:45	25.3	13:45	24.9	13:50	23.2	13:50
Soil bottom	-	-	24.7	14:40	24.0	14:45	22.8	15:00
Water reservoir	-	-	24.6	14:40	23.8	15:15	22.7	21:45
Drainage	-	-	23.4	17:00	22.6	18:00	22.6	22:25
Root barrier	-	-	22.8	17:35	22.5	19:20	22.4	22:45
Ceiling	22.4	23:25	22.6	00:15	23.0	00:00	22.5	23:45

4.3. Comparison of the Temperature Damping Effect of Substrate Layers

The temperature damping effect of the substrate layers during downward heat transfer is a critical factor in the thermal performance of roof systems. This effect refers to the reduction in temperature amplitude as heat travels through the substrates. The performance is influenced by a complex interplay of the substrate's characteristics, e.g., the depth and thermal capacity. For the green roof, moisture content, structure, specific composition, etc., relate. However, the thermal properties of some substrate layers of the green roof are not available. In the future, precise measurement of the thermal properties of those substrates can be carried out to support heat transfer analysis.

Figure 16 shows the temperature damping effect of the substrate layers on a typical summer sunny day, which indicates the comparative thermal performance of different roofing systems. In terms of overall thermal damping effectiveness, all roof systems outperform the conventional roof significantly. Green roof-plot C demonstrates the highest damping effect, followed by green roof-plot B, A and the cool roof. The advantage of green roofs stems from the multi-layer strategy that combines evapotranspiration, insulation and thermal mass.

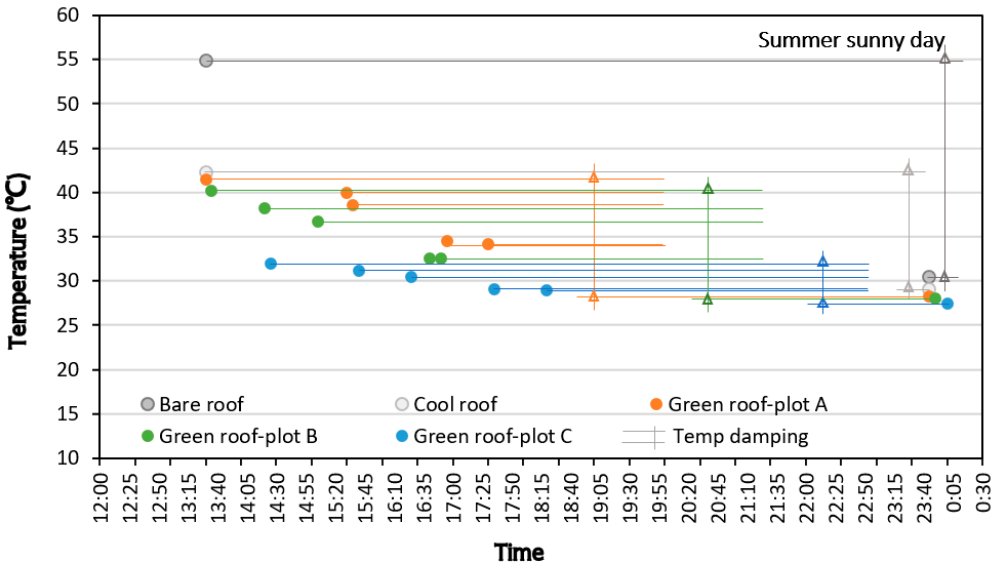


Figure 16. The temperature damping effect of substrate layers on a typical summer sunny day.

The temperature damping effect of the substrate layers during downward heat transfer on a summer sunny day is summarized in Table 8. For the conventional roof, its entire damping effect comes from the roof construction. Even through it has an insulation layer, it is also susceptible to heat transfer. For the cool roof, its thermal damping effect comes almost entirely from the white paint, i.e., the high-reflective coating. The temperature damping effectiveness of the cool roof was 13.2 °C, suggesting the coating effectively prevents heat from reaching the construction. Green roofs distribute the damping effect across multiple functional layers, creating a more robust and effective barrier. The thermal damping effectiveness of each substrate in the three green roof systems kept consistent as follows: drainage > soil > water reservoir > root barrier. The damping effect of the cool roof is attributed solely to the white paint, i.e., the high-reflective coating, whilst the efficiency of the green roof comes from the cumulative effect of multiple layers.

Table 8. The temperature damping effect of substrate layers during downward heat transfer through roof systems on a typical summer sunny day.

Substrate Layer	Cool Roof	Green Roof -Plot A	Green Roof -Plot B	Green Roof -Plot C
Soil/White paint	13.2	1.6	2	0.9
Water reservoir	-	1.3	1.5	0.6
Drainage	-	4.1	4.2	1.4
Root barrier	-	0.3	0	0.2

Figure 17 shows the temperature damping effect of the substrate layers on a typical summer rainy day, which indicates the comparative thermal performance of different roofing systems. In general, the overall comparative performance was similar to a summer sunny day. In terms of overall thermal damping effectiveness, all roof systems outperform the conventional roof significantly. Green roof-plot C demonstrates the highest damping effect, followed by green roof-plot B, green roof-plot A, and the cool roof. The efficiency of the green roof system comes from the cumulative effect of multiple layers.

The temperature damping effect of the substrate layers during downward heat transfer on a summer rainy day is summarized in Table 9. The trend was generally the same as on a summer sunny day. For the conventional roof, its entire damping effect comes from the roof construction. For the cool roof, its thermal damping effect is attributed solely to the white paint, i.e., the high-reflective coating. The temperature damping of the cool roof was 2.9 °C. The multi-layer strategy of green roofs creates a robust thermal buffer. The thermal damping effectiveness delivered by the different substrates in the three green roof systems was different. For green roof plot A, the comparative performance was drainage > soil = root barrier > water reservoir; for green roof plot B, the comparative performance was drainage > soil > water reservoir > root barrier; for green roof plot C, the comparative performance was soil > root barrier = drainage = water reservoir. This is mainly because, on a summer rainy day, the outermost layer of the roof systems comes as the cooling front, which may result in bidirectional heat transfer.

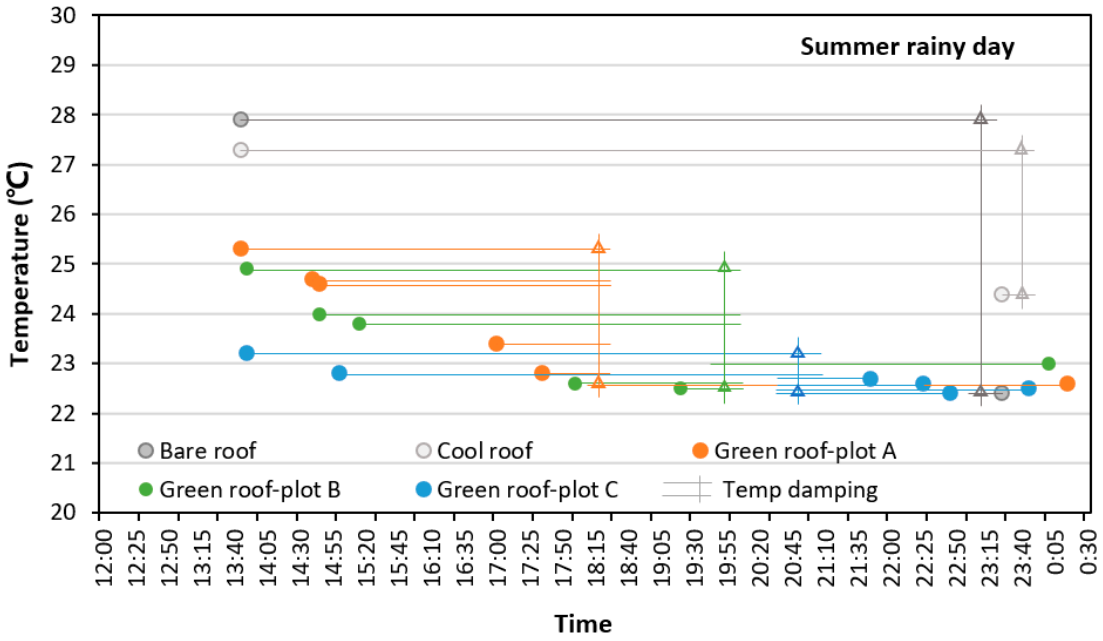


Figure 17. The temperature damping effect of substrate layers on a typical summer rainy day.

Table 9. The temperature damping effect of substrate layers during downward heat transfer through roof systems on a typical summer rainy day.

Substrate Layer	Cool Roof	Green Roof -Plot A	Green Roof -Plot B	Green Roof -Plot C
Soil/White paint	2.9	0.6	0.9	0.4
Water reservoir	-	0.1	0.2	0.1
Drainage	-	1.2	1.2	0.1
Root barrier	-	0.6	0.1	0.2

On a sunny day, the thermal dampening effectiveness of each substrate in the three green roofs is consistent. However, on a rainy day, there is no consistent pattern. This is mainly because the outmost layer of green roof systems may come as the cooling front, together with the complex cooling rate of multiple substrates (water reservoir and drainage may serve as an insulator), and bidirectional heat transfer may occur. Thermal lag and moisture dynamics dilute the layer-wise damping effect.

5. The Cooling Potential of the Cool Roof and Green Roof

5.1. Albedo of Different Roof Surfaces

The albedo values for the different roof surfaces are listed in Table 10. The measured albedo value of the conventional roof was 0.3. The cool roof demonstrated a relatively higher albedo of 0.58, which guaranteed its ability to reflect solar radiation.

Table 10. On-site measured values of albedo (α) for different roof surfaces.

Surface Type	α
Conventional roof	0.30
Cool roof	0.58
Green roof-plot A	0.27
Green roof-plot B	0.25
Green roof-plot C	0.22

5.2. The Diurnal Temperature Variation

5.2.1. Cool Roof

Figure 18 presents the diurnal temperature variations of the rooftop and underneath ceiling surfaces for the conventional roof and cool roof. The cool roof significantly lowers temperatures at both the outer surface and the inner ceiling surface compared to the conventional roof throughout the diurnal cycle. This demonstrates its effective solar reflectance and thermal emittance properties. On a summer sunny day, the concrete tile surface temperature of the conventional roof exhibited extreme fluctuations and peaked at 55.6 °C around midday. The cool roof surface temperature remained lower and more stable. Its peak temperature stayed at 42.3 °C. The temperatures at the ceiling surfaces were significantly lower and more attenuated than the corresponding rooftop temperatures, which averaged 30.3 °C and 28.3 °C for the conventional and cool roof, respectively. The cool roof greatly reduced the amplitude of temperature variation for both rooftop and ceiling surface temperatures.

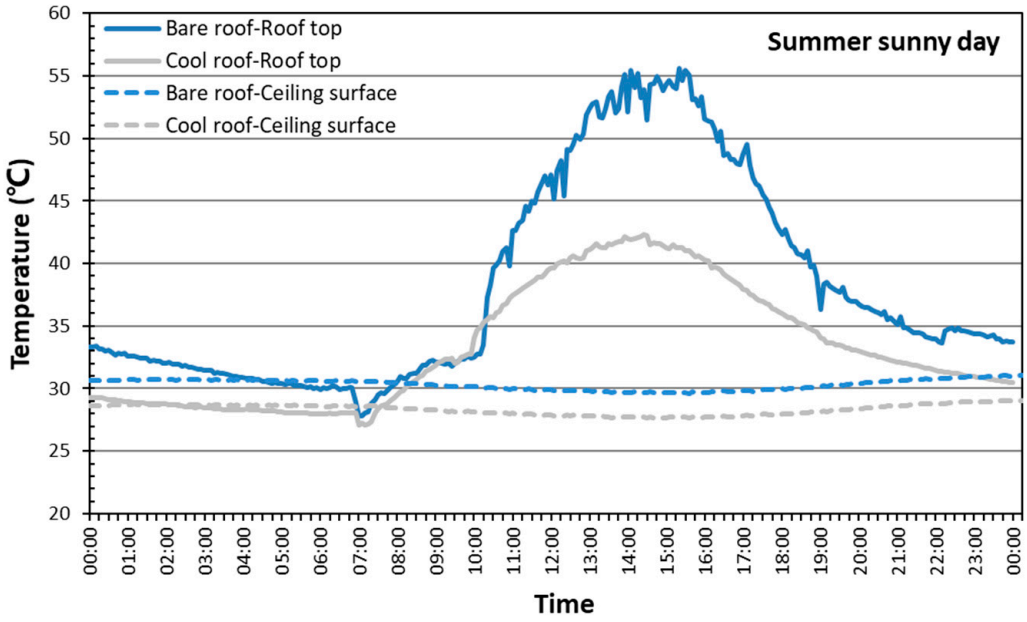


Figure 18. Diurnal temperature variation of the concrete/white paint top and underneath ceiling surfaces for the conventional roof and cool roof on a typical summer sunny day.

Figure 19 presents the diurnal temperature variations of the rooftop and underneath ceiling surfaces for the conventional roof and cool roof. On a rainy day, all measured temperatures were constrained within a narrow band. This is mainly because the solar radiation, the primary driver of daytime heating, is subdued due to cloud cover and precipitation. The concrete tile surface temperature rose from 24.4 °C in the early morning to a peak of about 30.1 °C around midday, while the cool roof remained relatively stable, with a maximum rooftop surface temperature of 27.3 °C. The ceiling surface temperatures of the conventional roof and cool roof fluctuated little, were nearly identical and averaged 24.3 °C and 24.1 °C, respectively. Although it shows a certain cooling benefit on the rooftop, it was almost eliminated at the interior ceiling. The thermal environment was governed more by ambient conditions. Its high albedo surface prevented significant heat absorption even from the diffuse light on a rainy day. The cool roof's effectiveness is highly weather-dependent.

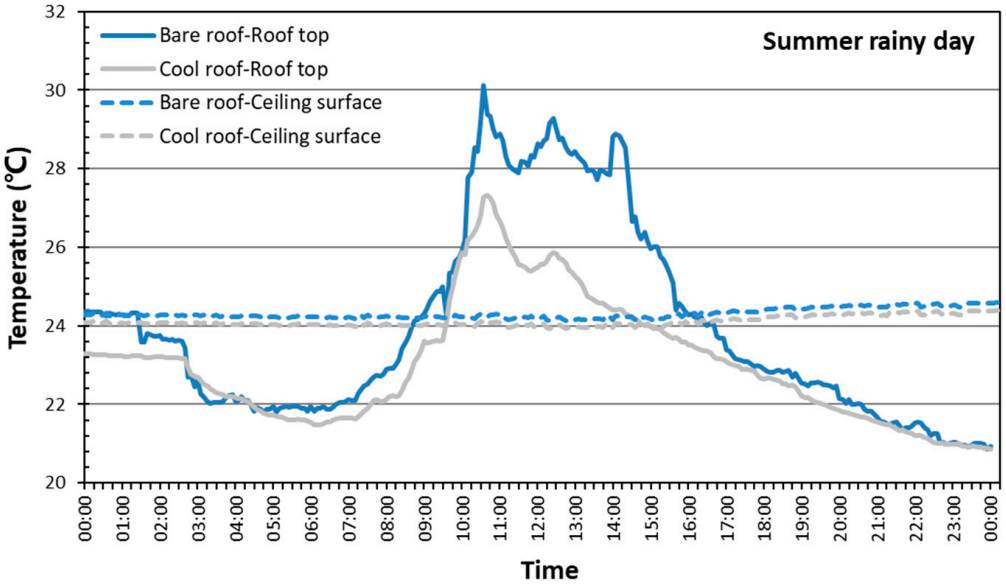


Figure 19. Diurnal temperature variation of the concrete/white paint top and underneath ceiling surfaces for the conventional roof and the cool roof on a typical summer rainy day.

5.2.2. Green Roof

Figure 20 demonstrates the diurnal temperature variations of the rooftop and underneath ceiling surfaces for the conventional and green roof plots. On a typical summer sunny day, the concrete tile surface temperature of the conventional roof remained the highest one nearly throughout the whole day compared to the three green roof plots. Large solar energy input heated up the conventional rooftop gradually, which peaked at 54.9 °C. The maximum temperatures of the soil surfaces were 41.5 °C, 40.2 °C and 32 °C for green roof-plots A, B and C, respectively. Higher vegetation coverage contributed significantly to this temperature reduction. The green canopy excludes a certain amount of solar radiation incident on the soil top, while evapotranspiration also plays an important role in dissipating heat. Moreover, the conventional roof and the three green roof plots all reached the highest temperatures between 13:00 and 15:00, generally at the same pace. The temperature variations responded vividly to environmental weather conditions, especially the solar radiation intensity.

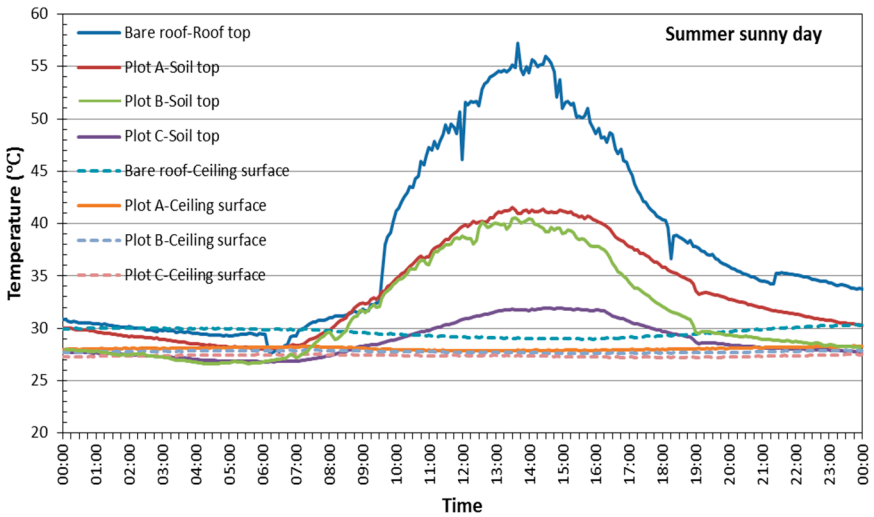


Figure 20. Diurnal temperature variation of the concrete/soil top and underneath ceiling surfaces for the conventional roof and the green roof plots on a typical summer sunny day.

The corresponding average ceiling surface temperatures were 29.6 °C, 28.1 °C, 27.8 °C and 27.4 °C for the conventional roof and the three green roof plots, respectively. It was in accordance with the corresponding amount of heat absorption on the rooftop that can be transmitted downwards. As a whole, plot C behaved the best in thermal damping aspect, followed by plots B and A.

Figure 21 shows the diurnal temperature variation of the rooftop and underneath ceiling surfaces on a typical summer rainy day. The daily maximum temperature of the concrete tile and soil tops of the three green roof plots were 27.9 °C, 25.3 °C, 24.9 °C and 23.2 °C, respectively. The conventional roof absorbed the largest amount of heat, followed by green roof-plots A, B and C. The gradually decreased peak amplitude can also be attributed to the higher vegetation cover. Similarly, the temperature fluctuations followed closely with the ambient environment.

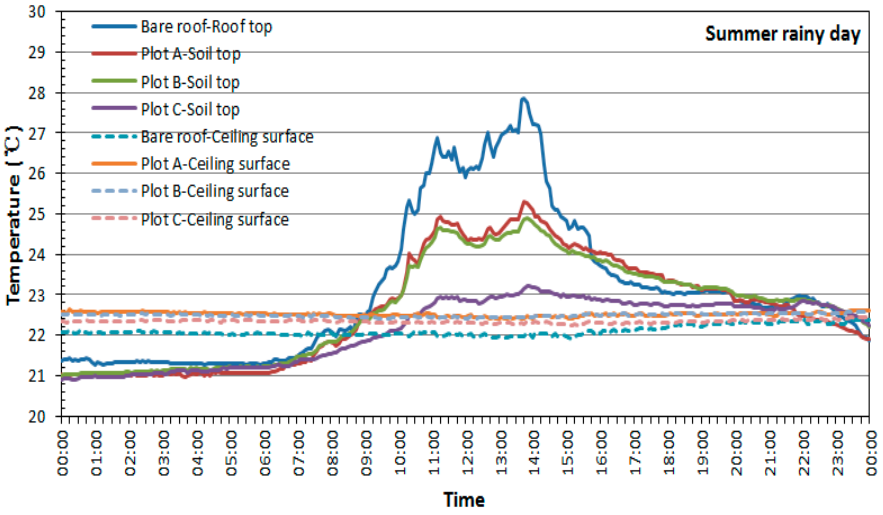


Figure 21. Diurnal temperature variation of the soil/concrete top and underneath ceiling surfaces for the conventional roof and the green roof plots on a typical summer rainy day.

The corresponding average ceiling surface temperatures were 22.1 °C, 22.5 °C, 22.4 °C and 22.3 °C for the conventional roof and the three green roofs, respectively. Plot A gained the highest ceiling surface temperature, followed by plots B and C and the conventional roof. The conventional roof absorbed the largest amount of heat but resulted in the lowest ceiling surface temperature. Without an additional thermal insulation layer (i.e., the multiple substrates including soils), it displayed higher cooling rates caused by rainfall. Generally, plot C still demonstrated the largest heat mitigation potential, followed by plots B and A.

Both on a summer sunny and rainy day, the daily maximum temperature of the top substrates and diurnal variation ranges all decreased gradually in the sequence of the conventional roof, the green roof-plots A, B and C. As such, the thermal damping capacity and the heat mitigation potential were in the sequence of green roof-plot C, green roof-plot B, green roof-plot A and the conventional roof.

5.3. Comparison of the Cooling Potential of the Cool Roof and Green Roof

The daily maximum surface temperature reduction (SDMR), which directly reflects the roof's ability to lower the roof surface temperature, is a key determinant of a roof's overall thermal performance. SDMR was selected as the cooling potential indicator of the different roof systems. The maximum value indicates the greatest potential. It is a comparison between conventional roof and advanced roof systems, which enables the comparability in an indirect way. As shown in Table 11, on a summer sunny say, the cooling potential (SDMR) on the concrete tile of the best performing system GR_C was 26 °C. This

was closely followed by the SDMR on the concrete tile of the GR_B, GR_A and CR, with 22.4 °C, 20.7 °C and 13.3 °C, respectively. The green roof systems demonstrated large advantages in SDMR, especially GR_C. The SDMR on the ceiling ranked as GR_C, GR_B, GR_A and CR, with 2.9 °C, 2.4 °C, 2.1 °C and 2.1 °C, separately. SDMR on the ceiling of GR_A was equivalent to CR, which can be attributed to the convective heat release towards outdoor spaces. The lower SDMR on the concrete tile contributed to the lower SDMR on the ceiling, which denoted a lower amount of heat transfer into indoor spaces and large cooling potential. The green roofs, particularly GR_C, provided the most significant reduction in peak surface temperature. The cool roof also showed a large cooling potential.

Table 11. The daily maximum surface temperature reduction (SDMR, in °C) of the different roof systems versus the conventional roof.

Typical Weather Condition	SDMR	BR-CR	BR-GR_A	BR-GR_B	BR-GR_C
Summer sunny day	Concrete tile	13.3	20.7	22.4	26
	Ceiling	2.1	2.1	2.4	2.9
Summer rainy day	Concrete tile	2.8	5.1	5.4	5.5
	Ceiling	0.2	−0.2	−0.6	−0.1

Notes: BR is the abbreviation for conventional roof; CR is the abbreviation for cool roof; GR_A is the abbreviation for green roof-plot A, planted with Zoysia Japonica; GR_B is the abbreviation for green roof-plot B, planted with Ophiopogon Jaburan; GR_C is the abbreviation for green roof-plot C, planted with Duranta Repens.

On a summer rainy day, the SDMR on the concrete tile of the best performing system GR_C was 5.5 °C, followed by GR_B, GR_A and CR, with 5.4 °C, 5.1 °C and 2.8 °C, separately. The green roof systems still demonstrated a large cooling potential in SDMR on a summer rainy day, especially GR_C. On rainy days, the cooling effect is still present but greatly diminished, as the driving force (solar heat gain) is reduced and rainwater provides natural cooling for all roof systems. For all green roofs (GR_C, GR_A, GR_B), the SDMR on the ceiling was slightly negative (−0.1 °C, −0.2 °C and −0.6 °C, separately). The cool roof presented a 0.2 °C SDMR. This phenomenon indicated that, on a rainy day, the underneath ceiling was slightly warmer than the BR. The insulative property of the green roof's substrate layers (soil, drainage) becomes the dominant factor. This insulation may slow down the release of residual heat from the building interior to the cooler outdoor environment, resulting in a minimally higher interior surface temperature compared to a conventional roof that may lose heat slightly faster. This would be beneficial in winter. Additionally, limited evapotranspiration (water reservoir, drainage), combined with the influence of thermal mass (soil), resulted in heat being released gradually. This constitutes a "warming effect at the ceiling". The reduced solar heat gain caused by the highly reflective coating, together with the natural cooling of rainwater, results in the lower ceiling surface temperature of CR.

6. Conclusions

An experimental investigation on the performance of a cool roof and green roof was conducted. The thermal behavior and cooling potential comparison were investigated during typical summer conditions in hot–humid climate. The main findings are listed as follows.

(1) Generally, the diurnal temperature profiles of the substrate layers were closely related to the corresponding meteorological conditions in terms of ambient air temperature and solar radiation. The cool roof and green roof can effectively reduce the rooftop surface temperature. Associated with the downward heat transfer process on a sunny

day, a "vertical thermal sequence" in peak temperatures of each substrate layer can be observed for the conventional, cool and green roofs. The temperature peaks were gradually shifted towards a later time with a lower value. However, on a rainy day, caused by possible heat release of the outermost layer, a local reversion in the thermal sequence may occur. The ceiling surface temperature may surpass those above the substrates. For the cool roof, a similar vertical thermal sequence happens. Performances of the cool roof and green roofs were closely related to environmental weather conditions and the corresponding physical properties of construction.

(2) The temperature damping effect of the substrate layers during downward heat transfer is a critical factor in the thermal performance of roof systems. Green roof plot C demonstrates the highest damping effect, followed by plots B and A and the cool roof, during both sunny and rainy conditions. The damping effect of the cool roof is attributed solely to the white paint, i.e., the high-reflective coating, whilst the efficiency of the green roof comes from the cumulative effect of multiple layers. On a sunny day, the thermal dampening effectiveness of each substrate in the three green roofs is consistent as follows: drainage > soil > water reservoir > root barrier. However, on a rainy day, there is no consistent pattern. This is mainly because the outermost layer of the green roof systems may come as the cooling front, and together with the complex cooling rate of multiple substrates, bidirectional heat transfer may occur.

(3) The albedo of the established cool roof in the experiment was 0.58. In terms of the diurnal temperature variation of the cool roof on a summer sunny day, the concrete tile surface temperature of the conventional roof exhibited extreme fluctuations and peaked at 55.6 °C around midday, while the rooftop surface temperature of the cool roof remained more stable, with a peak temperature staying at 42.3 °C. The temperatures at the ceiling surfaces were significantly lower and more attenuated than the corresponding rooftop temperatures, which averaged 30.3 °C and 28.3 °C for the conventional and cool roof, respectively. On a summer rainy day, the rooftop surface temperature peaked at 30.1 °C and 27.3 °C for the conventional and cool roof. The ceiling surface temperatures of the conventional roof and cool roof fluctuated little and were nearly identical, which averaged 24.3 °C and 24.1 °C, separately. On a summer sunny day, the cool roof greatly reduced the amplitude of the temperature variation for both the rooftop and ceiling surface temperatures throughout the diurnal cycle. On a rainy day, although the cool roof prevented significant heat absorption because of the high albedo surface, the cooling benefit was almost eliminated at the interior ceiling. In this weather condition, the thermal environment is more governed by ambient conditions and the envelop thermal properties. The cool roof's effectiveness is highly weather-dependent.

(4) The diurnal temperature variations of the green roof responded vividly to environmental weather conditions, especially the solar radiation intensity. On a sunny day, large solar energy input heated up the conventional rooftop gradually, which peaked at 54.9 °C. The maximum temperatures of the soil surfaces were 41.5 °C, 40.2 °C and 32 °C for green roof-plots A, B and C, respectively. The corresponding average ceiling surface temperatures were 29.6 °C, 28.1 °C, 27.8 °C and 27.4 °C for the conventional roof and the three green roof plots, respectively. On a rainy day, the daily maximum temperature of the concrete tile and soil tops of the three green roof plots were 27.9 °C, 25.3 °C, 24.9 °C and 23.2 °C, respectively. The corresponding average ceiling surface temperatures were 22.1 °C, 22.5 °C, 22.4 °C and 22.3 °C for the conventional roof and the green roofs, respectively. Both on a summer sunny and rainy day, green roof-plot C demonstrated the largest heat mitigation potential, followed by plot B and plot A. Distinct heat mitigation potential was closely related to the characteristics of

vegetation. Denser vegetation cover correlated to stronger thermal damping capacity and thus would contribute to larger heat mitigation potential.

(5) The daily maximum surface temperature reduction (SDMR), which directly reflects the roof's ability to lower the roof surface temperature, is a key determinant of a roof's overall thermal performance. On a summer sunny day, the cool roof and green roof showed significant cooling potential. SDMR on the concrete tile of the best performing system was 26 °C for GR_C, followed by GR_B, GR_A and CR, with 22.4 °C, 20.7 °C and 13.3 °C, respectively. The SDMR on the ceiling ranked as GR_C, GR_B, GR_A and CR, with 2.9 °C, 2.4 °C, 2.1 °C and 2.1 °C, separately. Lower SDMR on the concrete tile contributed to the lower SDMR on the ceiling, which denoted a lower amount of heat transfer into indoor spaces and large cooling potential.

(6) On a summer rainy day, the cooling effect was still present but greatly diminished. SDMR on the concrete tile of the best performing system GR_C was 5.5 °C, followed by GR_B, GR_A and CR, with 5.4 °C, 5.1 °C and 2.8 °C, separately. For all green roofs (GR_C, GR_A, GR_B), the SDMR on the ceiling was slightly negative (−0.1 °C, −0.2 °C and −0.6 °C, separately). The cool roof presented a 0.2 °C SDMR. A critical insight of a "warming effect at the ceiling" of the green roof on a rainy day was revealed. On rainy days, the insulation property of the green roof's substrates may slow down the release of heat from the interior to the cooler outdoor environment, resulting in a minimally higher interior surface temperature compared to the conventional roof that may lose heat slightly faster. The cooling benefit of the green roof functions primarily through evapotranspirative cooling and shading on a sunny day, while the thermal insulation property on a rainy day is noteworthy.

Overall, this study provides comprehensive empirical data on the thermal behavior of a cool roof and green roof in hot–humid subtropical climate during typical weather conditions. The holistic cooling potential investigation reveals a complex mechanism of different roof systems. Characterization of the comparative cooling potential provides a basis for optimization and prioritization. It offers critical insights for unlocking rooftop cooling potential, endorsing cool roof and green roof as pivotal solutions for urban heat mitigation and sustainable urban environments.

In the near future, thermal performance of cool roof and green roof in winter should be investigated to thoroughly evaluate the year-round benefits in subtropical climate. The cooling benefits in summer and insulation challenges in winter need to be properly balanced to enhance climate-based efficient design.

Author Contributions: T.Z.: Conceptualization; Methodology; Software; Validation; Data curation; Formal analysis; Investigation; Resources; Data curation; Writing—original draft; Writing—review and editing; Visualization; Supervision; Project administration; Funding acquisition. K.F.F.: Resources; Writing—review and editing; Supervision; Project administration. T.T.C.: Resources; Supervision. All authors have read and agreed to the published version of the manuscript.

Funding: This work was funded by R&D Program of Beijing Municipal Education Commission: KM202410005006.

Institutional Review Board Statement: Not applicable.

Data Availability Statement: The original contributions presented in this study are included in the article. Further inquiries can be directed to the corresponding author.

Acknowledgments: The experiment carried out in this paper was supported by Campus Sustainability Projects of City University of Hong Kong.

Conflicts of Interest: The authors declare no conflicts of interest.

References

1. Baumüller, J.; Hoffmann, U.; Reuter, U. *Climate Booklet for Urban Development*; Ministry of Transport and Infrastuature: Stuttgart, Germany, 1992.
2. Santamouris, M. Heat island research in Europe: The state of the art. *Adv. Build. Energy Res.* **2007**, *1*, 123–150. [CrossRef]
3. Cui, L.; Shi, J. Urbanization and its environmental effects in Shanghai, China. *Urban Clim.* **2012**, *2*, 1–15. [CrossRef]
4. Oke, T.R. The energetic basis of the urban heat island. *Q. J. R. Meteorol. Soc.* **1982**, *108*, 1–24. [CrossRef]
5. Akbari, H.; Konopacki, S. Energy effects of heat-island reduction strategies in Toronto, Canada. *Energy* **2004**, *29*, 191–210. [CrossRef]
6. Hirano, Y.; Fujita, T. Evaluation of the impact of the urban heat island on residential and commercial energy consumption in Tokyo. *Energy* **2012**, *37*, 371–383. [CrossRef]
7. Radhi, H.; Sharples, S. Quantifying the domestic electricity consumption for air-conditioning due to urban heat islands in hot arid regions. *Appl. Energy* **2013**, *112*, 371–380. [CrossRef]
8. Xu, L.Y.; Xie, X.D.; Li, S. Correlation analysis of the urban heat island effect and the spatial and temporal distribution of atmospheric particulates using TM images in Beijing. *Environ. Pollut.* **2013**, *178*, 102–114. [CrossRef] [PubMed]
9. Santamouris, M.; Paraponiaris, K.; Mihalakakou, G. Estimating the ecological footprint of the heat island effect over Athens, Greece. *Clim. Change* **2007**, *80*, 265–276. [CrossRef]
10. Pantavou, K.; Theoharatos, A.; Mavrakis, M.; Santamouris, M. Evaluating thermal comfort conditions and health responses during an extremely hot summer in Athens. *Build. Environ.* **2011**, *46*, 339–344. [CrossRef]
11. Santamouris, M. Cooling the cities-A review of reflective and green roof mitigation technologies to fight heat island and improve comfort in urban environments. *Sol. Energy* **2014**, *103*, 682–703. [CrossRef]
12. Akbari, H.; Levinson, R.; Rainer, L. Monitoring the energy-use effects of cool roofs on California commercial buildings. *Energy Build.* **2005**, *37*, 1007–1016. [CrossRef]
13. Zoulia, I.; Santamouris, M.; Dimoudi, A. Monitoring the effect of urban green areas on the heat island in Athens. *Environ. Monit. Assess.* **2009**, *156*, 275–292. [CrossRef]
14. Zhou, X.; Deng, S.; Cui, Y.; Fan, C. Developing a co-benefits evaluation model to optimize greening coverage designs on university campuses in hot and humid areas. *Energy Build.* **2025**, *328*, 115214. [CrossRef]
15. Akbari, H.; Leanna, S.R. Urban Surfaces and Heat Island Mitigation Potentials. *J. Hum. Environ. Syst.* **2008**, *11*, 85–101. [CrossRef]
16. Zinzi, M. Cool materials and cool roofs: Potentialities in Mediterranean buildings. *Adv. Build. Energy Res.* **2010**, *4*, 201–266. [CrossRef]
17. Synnefa, A.; Santamouris, M. Advances on technical, policy and market aspects of cool roof technology in Europe: The Cool Roofs project. *Energy Build.* **2012**, *55*, 35–41. [CrossRef]
18. Santamouris, M. Using cool pavements as a mitigation strategy to fight urban heat island-A review of the actual developments. *Renew. Sustain. Energy Rev.* **2013**, *26*, 224–240. [CrossRef]
19. Santamouris, M.; Pavlou, C.; Doukas, P.; Mihalakakou, G.; Synnefa, A.; Hatzibiros, A.; Patargias, P. Investigating and analysing the energy and environmental performance of an experimental green roof system installed in a nursery school building in Athens, Greece. *Energy* **2007**, *32*, 1781–1788. [CrossRef]
20. Sfakianaki, A.; Pagalou, E.; Pavlou, K.; Santamouris, M.; Assimakopoulos, M.N. Theoretical and experimental analysis of the thermal behaviour of a green roof system installed in two residential buildings in Athens, Greece. *Int. J. Energy Res.* **2009**, *33*, 1059–1069. [CrossRef]
21. Berardi, U.; GhaffarianHoseini, A.; GhaffarianHoseini, A. State-of-the-art analysis of the environmental benefits of green roofs. *Appl. Energy* **2014**, *115*, 411–428. [CrossRef]
22. U.S. General Service Admistration. *The Benefits and Challenges of Green Roofs on Public and Commercial Buildings*; A Report of the United States General Service Administration; United States General Service Administration: Washington, DC, USA, 2011.
23. Jim, C.Y.; Tsang, S.W. Biophysical properties and thermal performance of an intensive green roof. *Build. Environ.* **2011**, *46*, 1263–1274. [CrossRef]
24. Jim, C.Y.; Tsang, S.W. Ecological energetics of tropical intensive green roof. *Energy Build.* **2011**, *43*, 2696–2704. [CrossRef]
25. Aleksejeva, J.; Voulgaris, G.; Gasparatos, A. Systematic review of the climatic and non-climatic benefits of green roofs in urban areas. *Urban Clim.* **2024**, *58*, 102133. [CrossRef]
26. Manso, M.; Inês, T.; Silva, C.M.; Cruz, C.O. Green roof and green wall benefits and costs: A review of the quantitative evidence. *Renew. Sustain. Energy Rev.* **2021**, *135*, 110111. [CrossRef]
27. Gago, E.J.; Roldan, J.; Pacheco-Torres, R.; Ordóñez, J. The city and urban heat islands: A review of strategies to mitigate adverse effects. *Renew. Sustain. Energy Rev.* **2013**, *25*, 749–758. [CrossRef]
28. Parizotto, S.; Lamberts, R. Investigation of green roof thermal performance in temperate climate: A case study of an experimental building in Florianópolis city, Southern Brazil. *Energy Build.* **2011**, *43*, 1712–1722. [CrossRef]

29. Shen, H.; Tan, H.; Tzempelikos, A. The effect of reflective coatings on building surface temperatures, indoor environment and energy consumption-An experimental study. *Energy Build.* **2011**, *43*, 573–580. [CrossRef]
30. Alexandri, E.; Jones, P. Ponds, green roofs, pergolas and high albedo materials; which cooling technique for urban spaces? In Proceedings of the 23rd Conference of Passive and Low Energy Architecture, Geneva, Switzerland, 6–8 September 2006.
31. Dwivedi, A.; Mohan Buddhiraju, K. Impact of green roof on micro climate to reduce Urban Heat Island. *Remote Sens. Appl. Soc. Environ.* **2018**, *10*, 56–69. [CrossRef]
32. Hui, D. Benefits and potential applications of green roof systems in Hong Kong. *Evaluation* **2006**, *11*, 12.
33. Chan, A.L.S.; Chow, T.T. Energy and economic performance of green roof system under future climatic conditions in Hong Kong. *Energy Build.* **2013**, *64*, 182–198. [CrossRef]
34. Jim, C.Y.; Peng, L.L.H. Weather effect on thermal and energy performance of an extensive tropical green roof. *Urban For. Urban Green.* **2012**, *11*, 73–85. [CrossRef]
35. Jin, C.; Bai, X.; Luo, T.; Zou, M. Effects of green Roofs' variations on the regional thermal environment using measurements and simulations in Chongqing, China. *Urban For. Urban Green.* **2018**, *29*, 223–237. [CrossRef]
36. Hien, W.N.; Yu, C. *Study on the Urban Heat Island in Singapore*; National University of Singapore: Singapore, 2002.
37. Hien, W.N.; Yok, T.P.; Yu, C. Study of thermal performance of extensive rooftop greenery systems in the tropical climate. *Build. Environ.* **2007**, *42*, 25–54. [CrossRef]
38. Yang, J.; Kumar, D.L.M.; Pyrgou, A.; Chong, A.; Santamouris, M.; Kolokotsa, D.; Lee, S.E. Green and cool roofs' urban Heat Island mitigation potential in tropical climate. *Sol. Energy* **2018**, *173*, 597–609. [CrossRef]
39. Banting, D.; Doshi, H.; Li, J.; Missios, P.; Au, A.; Currie, B.A.; Verrati, M. *Report on the Environmental Benefits and Costs of Green Roof Technology for the City of Toronto*; MPRA Paper; University Library of Munich: Munich, Germany, 2005.
40. Gaffin, S.; Rosenzweig, C.; Eichenbaum-Pikser, J.; Khanbilvardi, R.; Susca, T. *A Temperature and Seasonal Energy Analysis of Green, White, and Black Roofs*; Technical Report; Center for Climate Systems Research, Columbia University: New York, NY, USA, 2010.
41. Pompeii, I. *Assessing Urban Heat Island Mitigation Using Green Roofs: A Hardware Scale Modeling Approach*; Shippensburg University: Shippensburg, PA, USA, 2010.
42. Williams, N.S.; Rayner, J.P.; Raynor, K.J. Green roofs for a wide brown land: Opportunities and barriers for rooftop greening in Australia. *Urban For. Urban Green.* **2010**, *9*, 245–251. [CrossRef]
43. Ríos-Fern'andez, J.C. Thermal performance assessment of cool roofs on supermarkets through case analysis in 13 cities. *Eng. Constr. Archit. Manag.* **2022**, *29*, 739–754. [CrossRef]
44. Rosati, A.; Fedel, M.; Rossi, S. NIR reflective pigments for cool roof applications: A comprehensive review. *J. Clean. Prod.* **2021**, *313*, 127826. [CrossRef]
45. Tian, D.; Zhang, J.; Gao, Z. The advancement of research in cool roof: Super cool roof, temperature-adaptive roof and crucial issues of application in cities. *Energy Build.* **2023**, *291*, 113131. [CrossRef]
46. Wu, Y.; Zhao, H.; Sun, H.; Duan, M.; Lin, B.; Wu, S. A review of the application of radiative sky cooling in buildings: Challenges and optimization. *Energy Convers. Manag.* **2022**, *256*, 115768. [CrossRef]
47. Morales-Inzunza, S.; González-Trevizo, M.; Martínez-Torres, K.E.; Luna-León, A.; Tamayo-Perez, U.J.; Fernández-Melchor, F.; Santamouris, M. On the potential of cool materials in the urban heat island context: Scalability challenges and technological setbacks towards building decarbonization. *Energy Build.* **2023**, *296*, 113330. [CrossRef]
48. Rawat, M.; Singh, R.N. A Study on the Comparative Review of Cool Roof Thermal Performance in Various Regions. *Energy Built Environ.* **2021**, *3*, 327–347. [CrossRef]
49. Takebayashi, H.; Moriyama, M. Surface heat budget on green roof and high reflection roof for mitigation of urban heat island. *Build. Environ.* **2007**, *42*, 2971–2979. [CrossRef]
50. Yang, J.; Wang, Z.H.; Kaloush, K.E. Environmental impacts of reflective materials: Is high albedo a 'silver bullet' for mitigating urban heat island? *Renew. Sustain. Energy Rev.* **2015**, *47*, 830–843. [CrossRef]
51. Ramamurthy, P.; Sun, T.; Rule, K.; Bou-Zeid, E. The joint influence of albedo and insulation on roof performance: A modeling study. *Energy Build.* **2015**, *102*, 317–327. [CrossRef]
52. Sailor, D.J.; Elley, T.B.; Gibson, M. Exploring the building energy impacts of green roof design decisions–a modeling study of buildings in four distinct climates. *J. Build. Phys.* **2012**, *35*, 372–391. [CrossRef]
53. Zinzi, M.; Agnoli, S. Cool and green roofs. An energy and comfort comparison between passive cooling and mitigation urban heat island techniques for residential buildings in the Mediterranean region. *Energy Build.* **2012**, *55*, 66–76. [CrossRef]
54. Omidreza Saadatian, A.; Sopian, K.; Salleh, E.; Lim, C.H.; Safa Riffat, B.; Saadatian Elham, C.; Toudeshki Arash, D.; Sulaiman, M.Y. A review of energy aspects of green roofs, Renewable and Sustainable. *Energy Rev.* **2013**, *23*, 155–168. [CrossRef]
55. Jamei, E.; Chau, H.W.; Seyedmahmoudian, M.; Stojcevski, A. Review on the cooling potential of green roofs in different climates. *Sci. Total Environ.* **2021**, *791*, 148407. [CrossRef]
56. Del Barrio, E.P. Analysis of the green roofs cooling potential in buildings. *Energy Build.* **1998**, *27*, 179–193. [CrossRef]

57. Eumorfopoulou, E.; Aravantinos, D. The contribution of a planted roof to the thermal protection of buildings in Greece. *Energy Build.* **1998**, *27*, 29–36. [CrossRef]
58. Lazzarin, R.M.; Castellotti, F.; Busato, F. Experimental measurements and numerical modeling of a green roof. *Energy Build.* **2005**, *37*, 1260–1267. [CrossRef]
59. Jim, C.Y. Effect of vegetation biomass structure on thermal performance of tropical green roof. *Landsc. Ecol. Eng.* **2012**, *8*, 173–187. [CrossRef]
60. Jim, C.Y.; Peng, L.L.H. Substrate moisture effect on water balance and thermal regime of a tropical extensive green roof. *Ecol. Eng.* **2012**, *47*, 9–23. [CrossRef]
61. Niachou, A.; Papakonstantinou, K.; Santamouris, M.; Tsangrassoulis, A.; Mihalakakou, G. Analysis of the green roof thermal properties and investigation of its energy performance. *Energy Build.* **2001**, *33*, 719–729. [CrossRef]
62. Tsang, S.W.; Jim, C.Y. Theoretical evaluation of thermal and energy performance of tropical green roofs. *Energy* **2011**, *36*, 3590–3598. [CrossRef]
63. Saiz, S.; Kennedy, C.; Bass, B.; Pressnail, K. Comparative life cycle assessment of standard and green roofs. *Environ. Sci. Technol.* **2006**, *40*, 4312–4316. [CrossRef] [PubMed]
64. Susca, T.; Gaffin, S.R.; Dell'Osso, G.R. Positive effects of vegetation: Urban heat island and green roofs. *Environ. Pollut.* **2011**, *159*, 2119–2126. [CrossRef]
65. Ray, S.; Glicksman, L. Potential energy savings of various roof technologies. *ASHRAE Build.* **2010**, *11*, 1–12.
66. Planning Department. *Planing Statistics: Land Utilization in Hong Kong*; Hong Kong Government: Hong Kong, 2025.
67. Jim, C.Y. Heat-sink effect and indoor warming imposed by tropical extensive green roof. *Ecol. Eng.* **2014**, *62*, 1–12. [CrossRef]
68. Lam, J.C.; Li, D.H.W. An analysis of electricity end-use in air-conditioned office buildings in Hong Kong. *Build. Environ.* **2002**, *37*, 845–855. [CrossRef]
69. Cui, Y.; Zhou, X.; Fan, C.; Lin, H.; Deng, S. Application of physics-informed neural networks-based hybrid prediction models in campus thermal environment prediction. *Build. Environ.* **2025**, *287*, 113880. [CrossRef]
70. Hong Kong SAR. *Guidelines on Performance Based Building Energy Code*; Electrical and Mechanical Services Department: Hong Kong, 2007.
71. Hong Kong SAR. *BEAM Plus: Building Environmental Assessment Method for New Buildings, BEAM Society*; HKGBC: Hong Kong, 2012.
72. Hong Kong SAR. *Final Report: Study on Green Roof Application in Hong Kong*; Urbis Limited; Architectural Services Department: Hong Kong, 2007.
73. Hui, S.C.M. *Final Report: Study of Thermal and Energy Performance of Green Roof Systems*; Department of Mechanical Engineering, The University of Hong Kong: Hong Kong, 2009.
74. *ISO 9060:1990*; Solar Energy—Specification and Classification of Instruments for Measuring Hemispherical Solar and Direct Solar Radiation. International Organization for Standardization: Geneva, Switzerland, 1990.
75. *ASTM E1918-06*; Standard Test Method for Measuring Solar Reflectance of Horizontal and Low-Sloped Surfaces in the Field. American Society for Testing and Materials: West Conshohocken, PA, USA, 2015.
76. Akbari, H.; Konopacki, S.J.; Eley, C.N.; Wilcox, B.A.; Van Geem, M.G.; Parker, D.S. Calculations for reflective roofs in support of standard 90.1. *ASHRAE Trans.* **1998**, *104*, 976–987.
77. *ASHRAE Standard 90.1-2022*; Energy Standard for Sites and Buildings Except Low-Rise Residential Buildings. ASHRAE: Atlanta, GA, USA, 2022.

Disclaimer/Publisher's Note: The statements, opinions and data contained in all publications are solely those of the individual author(s) and contributor(s) and not of MDPI and/or the editor(s). MDPI and/or the editor(s) disclaim responsibility for any injury to people or property resulting from any ideas, methods, instructions or products referred to in the content.